We would like to thank the reviewer for his useful comments and suggestions. We agree with the reviewer that a concrete terminology is required to deliver information in a scientific manuscript and to describe the biogeochemical cycle of compounds in the marine environment. This is sometimes difficult when a large environmental data set with similar parameters is presented and when different scientific fields use the same terminology for processes or species that are different. However, with this revised version we hope to have eliminated all subjects of concern and confusion. For example, we reduced the terminology of particles to biogenic, authigenic and lithogenic (removed terrigenous), describe each terms applied early in the manuscript and used them throughout the manuscript. Furthermore, we included a new table showing the different elemental ratios of the different particle sources.
Please find our comments below in italics. Below our comments, we included the revised manuscript and the supplementary material with word track changes.

For example, the authors seem to use "lithogenic" or "terrigenous" to indicate poorly exchangeable abiotic mineral particles in general, because they are initially interested in distinguishing these types of particles from biogenic particles, whereas I use "lithogenic" and "terrigenous" to specifically mean weathered aluminosilicate material that have elemental ratios consistent with crustal averages, and further separate the general class of abiotic mineral particles into "lithogenic" (i.e. aluminosilicates) vs "authigenic and scavenged" classes based on elemental ratios of sample particles compared to crustal averages. There are, of course, terrigenous and lithogenic particles that have elemental ratios different than crustal averages, so it's not that my version is necessarily better, but I think that if the authors explicitly and clearly define their use and meaning of the words "lithogenic"/ "terrigenous" early in the manuscript, this will help to reduce confusion amongst the general readership about what they are talking about.
Comment: We agree with the reviewer and removed the term "terrigenious" from the manuscript and replaced it with "lithogenic".

Another source of confusion was the use of the word "scavenged". This could refer to surface adsorbed Fe, which would probably be readily exchangeable (i.e. bioavailable), but could also refer to authigenic precipitates ranging from rather labile oxyhydroxides that would be accessible by a weak leach to more aged hydroxides and oxides that are not. At various points in the manuscript, the higher Fe/Al ratios they see in suspended particles are referred to as scavenged Fe (e.g. section 3.1.2 lines 412-418) or lithogenic Fe (e.g. section 3.2.2 lines 548-550), depending on the way they are talking about these terms in each of these sections. They should pick a definition of "scavenged" and "lithogenic" that can be used consistently throughout the manuscript.
Comment: We inserted a new paragraph at the beginning of the RD section and introduce the term biogenic, authigenic (incl. scavenged), and lithogenic particle. This terminology was applied throughout the manuscript.

I also think it would help if the authors could come up with terminology to more clearly differentiate leachable particulate metals from their 25% HAc leach of their SAPS samples (LP) compared to the leachable particle metals from their total dissolvable seawater samples (LPun). They do define this in section 3.1.1, but in referring to these fractions in the text, they are both sometimes referred to as "leachable" particulate X, even though the former leach is poorly correlated with total particulates, but the latter leach is well correlated and used as a stand-in for total particulates. A more differentiated set of terminology to refer to each of these will further help to clarify.

Comment: We removed the "P" from "LP" and "RP", and we eliminated the term "particulate" throughout the text that referred to the leachable fraction of particles collected by SAPS. The term "leachable particulate fraction" referrers now to LPUn (unfiltered seawater), while "leachable fraction" and "refractory fraction" referrers to L and R (SAPS).

Below I highlight specific places where I think additional clarifications will help.

Figure 2 caption: recommend replacing "corresponds to the concentration lables of LPunFe" with "corresponds to the same axis as LPunFe" to clarify the meaning.
Comment: Changed as suggested.

Section 3.1.1
Lines 370-372 and Figure 2: The authors state that LPun concentrations "were slightly lower than the particulate fraction", but there are a few instances when LPun Fe exceeds PFe (e.g. deep stn 13, surface stn 18). As the authors note, these are different sampling approaches and pore sizes, so it's not unexpected, but the authors should acknowledge this with language to indicate that the LPun were *usually* lower than P.
Comment: We included "usually".

Lines 380-383: Ok, I understand now what the authors are doing by using LPun as an *indicator* of PFe. I transcribed the data from the tables and made a scatter plot of LPun Fe vs PFe and fit a regression to convince myself that they are indeed related (and they are), since it's not always obvious from looking at profiles, but this is a plot that they should include in the supplementals, reporting slope and R2, to justify the usage of LPun to indicate PFe.
Comment: We included a figure in the supplements showing LPUn vs. P for Fe, Mn, and Al (now Figure S1).

Lines 396-418: the clarifications added by the authors in the revised version help. I think these paragraphs could be made even clearer by stating at the outset that there are three potential origins to particles: lithogenic, biogenic, and authigenic (including scavenged), and then proceed to argue why the ratios indicate the importance of authigenic precipitation (or scavenging). Note that this is partly a matter of terminology, but what the authors call scavenged, or surface adsorbed, Fe and Mn may not be surface adsorbed to lithogenic or other particles in the traditional sense, but rather exist as discrete Fe and Mn oxyhydroxide mineral particles formed by authigenic precipitation.
I think it would be helpful in this and other discussions if the authors made a table summarizing the Fe/Mn, Fe/Al, and Mn/Al ratios for the particle pools that they talk about (crustal, sediments, suspended particles, fecal pellets, and phytoplankton).

	Fe/Mn	Fe/Al	Mn/Al
crustal	58.00	0.20	0.00345
sediments	51.50	0.34	0.00660
suspended	68.00	1.25	0.01838
fecal pellet	70.50	0.48	0.00681
phytoplankton	1.70		

I don't think the additions regarding titanium are necessary (lines 403-405), since the authors already have Al data, which is an adequate lithogenic tracer. I would, however, add a discussion of the ratio of

PMn/PAl as it relates to crustal averages (which shows that PMn is enriched relative to PAl in suspended particles compared to both sediments and the typical crustal average), as this illuminates what is going on with Mn too and gives context for what it means to normalize Fe to Mn, which I still don't really understand.
We included a new paragraph at the beginning of the RD section introducing the used terminology, biogenic, lithogenic, and authigenic. We added the process of surface scavenging to the authigenic term and changed that throughout the text. In addition we included a new Table (Table2) showing here the different ratios of the different particle pools. We removed Ti and included the PMn/PAl ratio in the text. Here now the explanation, why we are applying the Fe/Mn ratio. Usually we use the Fe/Mn ratio to differentiate between inorganic and organic Fe in marine particles. Both trace metals are incorporated in phytoplankton and bacteria cells. Phytoplankton Fe requirements are high, while Mn requirements are low, thus the intracellular Fe content is higher and the Fe/Mn ratio of phytoplankton cells is low (1.7). Such a low ratio we usually measure for the particulate fraction in open ocean surface seawater, thus we assume that the majority of Fe is part of biogenic fraction, intra- or extracellular. On the shelf, the load of lithogenic particles is much higher (more Mn), with the consequence that the Fe/Mn ratio is higher. This is described in chapter 3.1.2.
However, main objective of the paper is to highlight the Fe cycle in the dissolved and particulate fraction and to distinguish between organic and inorganic particulate Fe using the Fe/Al and Fe/Mn ratio as tracers. However, the Fe/Mn ratio of particles is altered by scavenging of DFe and DMn onto their surfaces. Assuming that both dissolved components are scavenged at the same time, MnO is re-dissolved by the process of photoreduction, thus reducing the amount of scavenged Mn (amount unknown) and increasing the Fe/Mn ratio with time from the start point 51.1 (sediment). However, extending the discussion why the Mn/Al ratio is different in the different inorganic particle fractions and thus highlighting the marine Mn cycle (photoreduction, scavenging) would for our opinion distract from the Fe story and did not deliver any new insight to the differentiation of organic and inorganic Fe particles.

I am also still puzzled as to why the correlations are so good between PFe, PMn, and PAl (Figure 3). I would not expect scavenging (oxidation, precipitation, hydrolysis, etc.) behavior to be the same for these three elements, so why do these correlate so well?
Commwent: Yes, the correlations of PFe, PMn, and PAl are very good. We were surprised as well when we saw that tight correlation for the first time. However, we showed with the HAc leaches that the majority of PFe, PMn, and PAl were refractory, meaning locked inside the crystal structure of the particle/mineral. We assume that processes such as oxidation, precipitation and hydrolysis did not affect the unaltered composition of the interior of sediment particles. And even when there is a layer of surface scavenged Fe that underwent the proposed processes, their overall contribution to total Fe content (e.g. alumosilicates, in equilibrium with Mn and Al) is very small (see particle leaches).

Section 3.1.3
Line 429: I suggest saying "enriched with surface bound and authigenic Fe"
Comment: We included " and authigenic".

Lines 457-464: The authors conclude that variability in the PFe/PAl ratio in various pools is explained by different contributions of biogenic material and Fe scavenged onto particles surfaces. The biogenic contribution is likely negligible, since Fe concentrations in phytoplankton is so much lower than in lithogenic and authigenic particles (lines 408-409). I agree that variations in the amount of scavenged and

authigenic Fe is important for the PFe/PAl ratio. Note that there are large variations in the PMn/PAl ratio too between the different particle pools (see table above), indicating that there is also variation in the scavenged/authigenic Mn, which makes interpreting the Fe/Mn difficult.
Comment: We agree with the reviewer and changed the sentence to "The observed variability in the PFe/PAl ratio in the various particle pools is therefore a consequence of different amounts of lithogenic and authigenic particles". Difficulties with the Fe/Mn ratio, see comments above.

The authors conclude that similar PFe/PMn in faecal pellets compared to suspended particles in the water column indicate that "Fe in krill faecal pellets was predominately associated with terrigenous material". Firstly, do they mean terrigenous as opposed to biogenic? If so, which terrigenous? From the molar ratios for all the pools (see table above), the ratios in faecal pellets seem most similar to sediments rather than to suspended particles, so it may be worth highlighting the similarity to sediments instead of comparing to suspended particles.
Comment: We agree with the reviewer that when taking the Mn/Al and the Fe/Al ratio into account mainly sediments were incorporated in faecal pellets. However, the Fe/Mn ratio suggests that suspended particles were incorporated in faecal pellets. Anyway, we turned the conclusion around, rewrote the sentences, and concluded that different amounts of lithogenic and authigenic particles are responsible for the variability of the elemental ratios.

Section 3.2.2
Lines 548-550: The authors conclude that the particulate trace metals were "mainly incorporated in lithogenic material", since the leachable fraction from a 25% HAc leach was so small. What do the authors mean here by "lithogenic material", since elsewhere in the text, the authors argue that scavenging of DFe is responsible for increasing the Fe/Al and Fe/Mn in suspended particles compared to sediment and crustal averages (lines 412-418), and that scavenged Fe is exchangeable with DFe in the water column (lines 559-565). 25%HAc is a fairly weak leach, and there can still be authigenic minerals (hydroxides and oxides) that are not accessed by this leach, so do they mean that lithogenic material includes some of these hydroxides and oxides, or do they mean that the suspended particles have a lithogenic (aluminosilicate?) origin that has a much higher Fe/Al and Fe/Mn than the sediments and crustal averages? This point, though seemingly picky, is an example of how it would help to define their use of "lithogenic" more precisely.
Comment: We agree with the reviewer that "lithogenic" can mean a lot in this sense. However, we meant rock type minerals and replaced "lithogenic" by "mineral structures unaffected by a weak acid leach (e.g. aged oxyhydroxides and alumosilicates)".

Section 3.2.3
Lines 574-583: the description of the faecal pellet Fe flux is clear, but it would be useful to add in total particulate Fe excreted by krill (faecal pellet mass and % of total Fe that is leachable, so giving an indication of total Fe would complete the picture).
Comment: Table 5 shows the faecal pellet mass, how much total Fe is incorporated, and how much Fe is leachable in %. These results are based on krill incubation experiments. However, we included in the text, how much Fe (in µmol mg-1) was incorporated in faecal pellets and how much Fe (in nmol mg-1) on average is leachable.

Typos, wording, etc.
P.10, line 309: add *also*: “Unfiltered surface seawater samples were *also* collected and dispensed...”
Comment: We included “also”

Mechanisms of dissolved and labile particulate iron supply to shelf waters and phytoplankton blooms off South Georgia, Southern Ocean

Christian Schlosser[1,2,*], Katrin Schmidt[3,4], Alfred Aquilina[1], William B. Homoky[1,5], Maxi Castrillejo[1,6], Rachel A. Mills[1], Matthew D. Patey[1], Sophie Fielding[3], Angus Atkinson[7], and Eric P. Achterberg[1,2]

[1] Ocean and Earth Science, National Oceanography Centre Southampton, University of Southampton, SO14 3ZH Southampton, United Kingdom

[2] GEOMAR Helmholtz Centre for Ocean Research, Wischhofstr. 1-3, 24148 Kiel, Germany

[3] British Antarctic Survey, CB3 0ET Cambridge, United Kingdom

[4] School of Geography, Earth and Environmental Sciences, University of Plymouth, PL4 8AA Plymouth, United Kingdom

[5] Department of Earth Sciences, University of Oxford, OX1 3AN Oxford, United Kingdom

[6] Institut de Ciència i Tecnologia Ambientals & Departament de Física, Universitat Autònoma de Barcelona, 08193 Bellaterra, Spain

[7] Plymouth Marine Laboratory, Prospect Place, The Hoe, PL1 3DH Plymouth, United Kingdom

For submission to Biogeosciences

* Corresponding author Christian Schlosser (Email: cschlosser@geomar.de,
Phone: 0049 (0) 431 600 1297)

Abstract (~~369~~ 375 words)

The island of South Georgia is situated in the iron (Fe) depleted Antarctic Circumpolar Current of the Southern Ocean. Iron emanating from its shelf system fuels large phytoplankton blooms downstream of the island, but the actual supply mechanisms are unclear. To address this, we present an inventory of Fe, manganese (Mn) and aluminium (Al) in shelf sediments, pore waters and the water column in the vicinity of South Georgia, alongside data on zooplankton-mediated Fe cycling processes, and provide estimates of the relative dissolved Fe (DFe) fluxes from these sources. ~~The s~~Seafloor sediments, modified by authigenic Fe precipitation, were the main particulate Fe source to shelf bottom waters as indicated by the similar Fe/Mn and Fe/Al ratios for shelf sediments and suspended particles in the water column. Less than 1% of the total particulate Fe pool was leachable surface adsorbed (labile) Fe, and therefore potentially available to organisms. Pore waters formed the primary DFe source to shelf bottom waters supplying 0.1 – 44 μmol DFe m^{-2} d^{-1}. However, we estimate that only 0.41 ± 0.26 μmol DFe m^{-2} d^{-1} was transferred to the surface mixed layer by vertical diffusive and advective mixing. Other trace metal sources to surface waters included glacial flour released by melting glaciers and via zooplankton egestion and excretion processes. On average 6.5 ± 8.2 μmol m^{-2} d^{-1} of labile particulate Fe was supplied to the surface mixed layer via faecal pellets formed by Antarctic krill (*Euphausia superba*), with a further 1.1 ± 2.2 μmol DFe m^{-2} d^{-1} released directly by the krill. The faecal pellets released by krill included seafloor-derived lithogenic and authigenic material and settled algal debris, in addition to freshly ingested suspended phytoplankton cells.

The Fe requirement of the phytoplankton blooms ~1,250 km downstream of South Georgia was estimated at 0.33 ± 0.11 μmol m^{-2} d^{-1}, with the DFe supply by horizontal/vertical mixing, deep winter mixing and aeolian dust estimated as ~0.12 μmol m^{-2} d^{-1}. We hypothesize that a substantial contribution of DFe was provided through recycling of

biogenically stored Fe following luxury Fe uptake by phytoplankton on the Fe-rich shelf. This process would allow Fe to be retained in the surface mixed layer of waters downstream of South Georgia through continuous recycling and biological uptake, supplying the large downstream phytoplankton blooms.

1. Introduction

The Southern Ocean is the largest ‘High Nitrate Low Chlorophyll’ (HNLC) region of the global ocean (Buesseler et al., 2004), as a consequence of low iron (Fe) supply and subsequent reduced phytoplankton growth (Buesseler et al., 2004; Tsuda et al., 2009). Iron can be supplied to surface waters of the Southern Ocean by atmospheric dust inputs (Cassar et al., 2007; Gao et al., 2001), horizontal/vertical advective and diffusive mixing processes (de Jong et al., 2012), resuspension from shelf sediments (Kalnejais et al., 2010; Marsay et al., 2014), melting of icebergs and glaciers (Raiswell et al., 2008), and hydrothermal inputs (German et al., 2016). Despite the overall HNLC status of the Southern Ocean, regions in the wake of islands feature large seasonal phytoplankton blooms; the Fe sources to these blooms are however poorly constrained (de Jong et al., 2012; Planquette et al., 2007; Pollard et al., 2009).

Downstream of the island of South Georgia intense, long-lasting phytoplankton blooms have been observed which extend hundreds of kilometres, and require an enhanced Fe supply. The blooms peak in austral summer (Borrione et al., 2013), stretch over an area of ~ 750,000 km^2 (Atkinson et al., 2001; Korb et al., 2004), and are responsible for the largest dissolved inorganic carbon deficit reported within the Antarctic Circumpolar Current (ACC) (Jones et al., 2015; Jones et al., 2012). As a consequence of the Fe fertilisation, the waters in the vicinity of South Georgia support extensive phytoplankton blooms and a large biomass of zooplankton, fish, seabirds and marine mammals, some of which are exploited commercially (Atkinson et al., 2001; Murphy et al., 2007).

South Georgia forms part of the volcanically active Scotia Arc in the Atlantic sector of the Southern Ocean and is surrounded by a broad 30 to 100 km wide shelf with an average (albeit highly variable) depth of ca. 200 m (Fig. 1). The island is situated between the Antarctic Polar Front (PF) and the Southern ACC Front (SACCF), within the general northeast flow of the ACC (Meredith et al., 2005; Whitehouse et al., 2008). The ACC surface waters are enriched in nitrate, phosphate and silicic acid, but strongly depleted in most trace elements, notably Fe and manganese (Mn) (Browning et al., 2014). The large seasonal phytoplankton blooms downstream of South Georgia are thought to be supplied with Fe from the island during the passage of ACC waters (Borrione et al., 2013; Nielsdóttir et al., 2012).

In this study we provide the first comprehensive data set of dissolved and (labile) particulate Fe, Mn, and Al in sediments, pore waters, and the water column overlaying the shelf and shelf edge regions of South Georgia. We also include published data on the role of Antarctic krill in new Fe supply and recycling in this region (Schmidt et al., 2011; Schmidt et al., 2016). We discuss differences between the various analysed trace metal fractions and the supply routes of dissolved and (labile) particulate Fe, such as sedimentary pore water efflux, supply of sediment derived particulate Fe to the surface mixed layer, efflux of Fe from glacial melting and supply of Fe by faecal pellets of Antarctic krill. Furthermore, we discuss the productivity of the bloom region to the north of South Georgia in relation to the estimated Fe supply rates.

2. Methods

2.1 Cruises and Sampling

Samples were collected during three research cruises to South Georgia in 2011 (JR247, JC055), and 2013 (JR274). While cruises JR247 and JR274 aimed to examine the pelagic shelf ecosystem by collection of predominantly water samples (and zooplankton during JR247) on the northern shelf, JC055 explored solely the composition of sediments on the South Georgia shelf. Cruise JR247 took place in January 2011 on RRS *James Clark Ross*, and 14 sites on the northern shelf and shelf edge of South Georgia were visited (stations

1 – 21; Fig. 1). Suspended particles were collected on acid cleaned polycarbonate filters (1 µm pore size; Whatman) using in-situ Stand-Alone Pumping Systems (SAPS; Challenger Oceanic) attached to a Kevlar wire and deployed at 20 m, 50 m and 150 m depth (Fig. 1, red dots). The filters were rinsed with deionized water (Milli-Q; Millipore), stored at -20°C, and shipped frozen to the National Oceanography Centre Southampton (NOCS).

Subsurface seawater samples were collected by trace metal clean samplers (Ocean Test Equipment (OTE)) at 9 of the 14 SAPS locations (Fig. 1; black stars). Seawater samples were filtered using cartridge filter (0.2 µm Sartobran P300; Sartorius) into acid cleaned 125 mL low-density polyethylene (LDPE) bottles (Nalgene). Unfiltered samples were collected in 125 mL LDPE bottles for analysis of total dissolvable (TD) trace metals. Surface waters from the South Georgia shelf were collected using a tow fish deployed alongside the ship at 3 – 4 m depth. Samples were filtered in-line using a cartridge filter (0.2 µm Sartobran P300; Sartorius) and dispensed in acid washed 125 mL LDPE bottles. Unfiltered surface seawater samples were also collected and dispensed in acid washed 125 mL LDPE bottles. All seawater samples were acidified on-board with ultra clean HNO_3 (15 M UpA grade, Romil) to pH 1.7 (22 µmol H^+ L^{-1}). For a more detailed description of all sample-handling procedures, please see Supplementary Text S1.

In January and February 2013, RRS *James Clark Ross* cruise JR274 revisited South Georgia and collected surface seawater samples covering the shelf, shelf-edge, and open ocean areas around the island. Dissolved and TD trace elements in surface seawater samples were collected using the tow fish and treated similarly to samples from JR247. For a more detailed description of all sample-handling procedures, please see Supplementary Text S1.

During the RRS *James Cook* cruise JC055 in February 2011, a megacorer (Bowers and Connelly type) was used to collect surface sediment and pore water samples on the southern side of South Georgia (there was no opportunity to sample the northern side of the island). Cores representing the intact sediment – water interface were retrieved from three sites on the southern shelf, at water depths of ca. 250 m (S1 – S3) (Fig. 1, blue hexagons). Pore waters were separated by centrifugation under N_2 atmosphere and filtered using cellulose nitrate syringe filters (0.2 µm pore size; Whatman (Homoky et al., 2012). Conjugate sediments were freeze dried on board and stored at room temperature. A more detailed description of sediment and pore water sample-handling procedures is provided in Supplementary Text S2.

Krill faecal pellets were obtained during on-board krill incubations performed during JR247. Incubations were performed in darkness in the laminar flow cabinet at ambient surface layer temperature. The krill were incubated in filtered seawater from the tow fish for up to ~3 h immediately after capture, so that pellets obtained derived from material ingested in situ. These incubations and their results are described in more detail in Schmidt et al. (2016).

2.2 Trace metal analysis in suspended particles and krill faecal pellets

The labile trace metal fraction of suspended particles (SAPS) and krill faecal pellets, was remobilized using a 25% acetic acid solution (glacial SpA, Romil) following Planquette et al. (2011). The labile trace metal fraction is hereafter referred to as the leachable ~~particulate~~ trace metal fraction (L~~P~~). The remaining particles were digested on a hot plate applying a mixture of aqua regia and hydrogen fluoride (Planquette et al., 2011). This fraction will be referred to as the refractory ~~particulate~~ fraction (R~~P~~). The particulate trace metal fraction (P) is the sum of leachable ~~particulate~~ (L~~P~~) and refractory ~~particulate~~ (R~~P~~). All samples were analysed by collision cell inductively coupled plasma - mass spectrometry (ICP-MS) (ThermoFisher Scientific, XSeriesII). For more detailed description of measured certified reference material see Supplementary Text S1.

2.3 Trace metal analysis of seawater

The filtered and unfiltered seawater samples were stored for a period of 12 months prior to analysis. Concentrations of dissolved and total dissolvable Fe, Mn, and Al in seawater were determined by off-line pre-concentration and isotope dilution / standard addition ICP-MS (ThermoFisher Scientific Element2 XR) according to Rapp et al. (2017). For a more detailed description of the method and measured reference materials see Supplementary Text S1.

2.4 Trace metal analysis of pore waters and sediments

Sub-samples of the bulk, homogenized sediments were fully dissolved following an aqua regia and combined hydrofluoric/perchloric acid digestion method following Homoky et al. (2011). The acid digests and pore waters were analysed by ICP-optical emission spectrometry (OES) (Perkin Elmer Optima 4300DV). For a more detailed description of the method and measured reference materials see Supplementary Text S2.

3. Results & Discussion

3.1 Supply routes of suspended particulate Fe, Mn, and Al

To avoid confusion, we will now define the terms biogenic, lithogenic, and authigenic particles, as they will be used frequently in the following sections. Biogenic particles refer to suspended organic particles, living and dead, such as phytoplankton cells. Lithogenic particles comprise mineral fragments, such as glacial flour and sediment particles. Authigenic particle include surface-scavenged trace metals and secondary minerals, such as amourphous FeO(OH) (e.g. goethite), that are formed in seawater and because of their age are insoluble to weak acid leaches (e.g. 25% acetic acid solution).

3.1.1 Characterization of (the two) particulate trace metal fractions

Two different particulate fractions were obtained from samples collected during JR247; a particulate fraction from suspended particles collected using 1 µm pore size SAPS filters (P) and a leachable particulate fraction from unfiltered acidified seawater samples (LP_{Un}) collected at the same depth. LP_{Un} was calculated following Eq. (1):

$$LP_{Un} = \text{total dissolvable (TD; unfiltered)} - \text{dissolved (D; 0.2 µm filtered)} \qquad (1)$$

Because of the different sampling approaches (SAPS vs. OTE water samplers), filter sizes (>1 µm for SAPS vs. >0.2 µm for dissolved seawater) and digestion procedures (aqua regia + HF for SAPS particles vs. water sample storage at pH 1.7 [22 µmol H^+ L^{-1}]), concentrations of LP_{Un} and P differed, but showed similar distribution patterns in the water column (Fig. 2 and S1, Table 1 and 2). The concentrations of Fe, Mn and Al in the LP_{Un} fraction (LP_{Un}Fe, LP_{Un}Mn, LP_{Un}Al) were usually slightly lower than the particulate fraction from suspended particles (PFe, PMn, PAl). The LP_{Un} of unfiltered seawater samples corresponded to ~ 63 ± 4 % of the PFe, 83 ± 11% of the PAl and nearly 100 ± 10% of the PMn fractions obtained by SAPS. The average LP_{Un} trace metal ratios (LP_{Un}Fe/ LP_{Un}Mn = 33.07 ± 3.45 (1 σ) and LP_{Un}Fe/ LP_{Un}Al = 0.65 ± 0.10 (n=69)), were about half of the elemental ratios of suspended particles obtained by SAPS (PFe/PMn = 68.0 ± 0.6 and PFe/PAl = 1.251 ± 0.042 (n=42) (Fig. 3; Table 1~~ and ~~, 2 and 3)).

The lower concentrations of Fe and Al and the reduced elemental ratios in the LP_{Un} compared to the P fractions suggests that an unknown fraction of particulate Fe and Al in seawater was not leached during the acidification procedure at pH 1.7 over 12 months. However, since P and LP_{Un} displayed similar trends with depth (Fig. 2 and S1), LP_{Un} was used in sections 3.1.3 and 3.3 as an indicator for the abundance of particulate trace metals at locations where particulate samples could not be retrieved by SAPS, e.g. in surface waters collected by the tow fish and depths greater than 150 m.

3.1.2 Suspended particulate trace metals in the water column

Concentrations of PFe, PMn and PAl in the water column ranged from 0.87 – 267 nmol L^{-1}, 0.01 – 3.85 nmol L^{-1}, and 0.60 – 195 nmol L^{-1}, respectively (Fig. 2, Table 2). Concentrations of $LP_{Un}Fe$, $LP_{Un}Mn$ and $LP_{Un}Al$ ranged from 1 – 118 nmol L^{-1}, 0.01 – 100 nmol L^{-1}, and 1 – 141 nmol L^{-1}, respectively (Fig. 2, Table 1). Below the isopycnal density layer 27.05 kg m^{-3}, located at ~50 – 70 m depth, P and LP_{Un} increased with depth and showed a maximum near the seafloor of e.g. 207 nmol L^{-1} for PFe and 112 nmol L^{-1} for $LP_{Un}Fe$ (#17, Table 2). Most sites on the shelf (bottom depth ≤ 260 m; #9/10, #13, #14, #17, and #21) showed seafloor maxima, in agreement with other shelf studies. For example, Milne et al. (2017) reported concentrations of up to 140 nmol L^{-1} for PFe and 800 nmol L^{-1} for PAl in bottom waters on the west African shelf, and Chase et al. (2005) showed bottom water maxima of up to 400 nmol L^{-1} for $LP_{Un}Fe$ off the Oregon coast.

Strong linear relationships between elements were observed for suspended particles (SAPS) obtained from above and below the 27.05 kg m^{-3} isopycnal, with elemental ratios of PFe/PMn = 68.0 ± 0.6~~ and~~, PFe/PAl = 1.25 ± 0.04 and PMn/PAl = 0.0171 ± 0.0041 (n=42) (Fig. 3, Table 2 and 3). These elemental ratios were higher than those reported for the earth's crust (Fe/Mn = 58.0, Fe/Al = 0.2, Mn/Al = 0.0035~~, Fe/Ti (titanium) = 9.1~~ (Wedepohl, 1995)) and sediment samples collected to the south of the island (mean sediment surface layer of S1, S2, S3; SFe/SMn = 51.5 ± 2.4, SFe/SAl = 0.34 ± 0.02, SMn/SAl = 0.0066 ± 0.0002 (Fig. 4, Table 3 and ~~3~~4)~~, and SFe/STi = 9.9 (not shown)~~), suggesting that the suspended particles were more enriched in Fe than crustal ~~lithogenic particles~~and lithogenic particles (Table 3). ~~We are aware that other trace metals, such as Ti, would be more appropriate than Mn to indicate the lithogenic origin of suspended particles. However, the element Ti was not monitored for dissolved, unfiltered seawater and particulate samples obtained by SAPS.~~

The Fe/Mn ratios among different phytoplankton species show strong variations but are typically much lower (Fe/Mn ~ 1.7 (Ho et al., 2003)), with also lower Fe concentrations than ~~terrestrial~~lithogenic~~/sediment~~ particles (cellular Fe concentration of phytoplankton ~ 0.7 mmol kg^{-1} (Ho et al., 2003); upper crust ~ 550 mmol kg^{-1} (Wedepohl, 1995)). A prevalence of biogenic particles in the suspended particle pool would be expected to result in reduced PFe/PMn ratios in our SAPS samples to values less than 51.5 as was observed in the sediments.

It is most likely that ~~scavenging of DFe onto suspended lithogenic/sediment particles~~ authigenic Fe precipitation (e.g. DFe was scavenged onto sediment particles) increased the Fe to Al (and Fe to Mn) ratio of suspended particles (PFe/PAl = 1.25; PFe/PMn = 68.0) compared to sediment particles (SFe/SAl = 0.34; SFe/SMn = 51.5). At seawater pH (~pH 8), dissolved Fe(III) is rapidly hydrolysed to soluble Fe(III)(OH)$_3$ (< 0.02 µm) which readily accumulates as nanometer sized colloids (0.02 – 0.2 µm) (Liu and Millero, 2002) and particles (> 0.2 µm) (own observation). It has been also shown that both soluble and colloidal Fe are attracted by charged surfaces (organic and inorganic particle surfaces), a process that removes DFe and simultaneously increases the amount of particulate Fe in seawater over time (Schlosser et al., 2011).

A range of mechanisms delivers suspended particles to the surface waters. These transport mechanisms will be discussed in the following section.

3.1.3 Glacial outflow and zooplankton feeding activity

While most stations on the shelf showed bottom water maxima of particulate metals, at three sampling sites located on the shelf (#18) and shelf edge (#15/16 and #19/20), the particulate trace metal concentrations featured maxima in the top 100 m of the water column (Fig. 2 and 5). At site #19/20, ca. 100 km away from the coast with a water depth of 1.741 m, the PFe concentration at 20 m depth was 97 nmol L^{-1}, similar to LP$_{Un}$Fe (Fig. 5). The elemental ratio PFe/PAl of these samples (e.g. 1.01 for site #19/20, 20 m depth) were close to the average ratio (PFe/PAl = 1.25), indicating that lithogenic and ~~lithogenic particles enriched with surface bound~~ authigenic Fe dominated the suspended particulate pool in these surface waters.

The surface water maxima of trace metals could have two supply routes: 1) lateral transport of waters containing lithogenic and authigenic particles from shallow island shelf sediments, and 2) transport of glacial particles following melt processes. The reduced salinities (~33.3 PSU) recorded in surface waters in Cumberland Bay and ~50 km offshore of South Georgia (~33.8) (Fig. 6(c) and ~~S1~~S2) provide an indication of glacial outflow, melting of icebergs and run-off of melt water streams. Enhanced LP$_{Un}$Fe concentrations of 2.2 µmol L^{-1} in low salinity surface waters inside Cumberland Bay, are indicative of a meltwater source (LP$_{Un}$ concentration used as only water samples from the tow fish available). The LP$_{Un}$Fe concentration decreased strongly with increasing distance from the coast, and exhibited an abrupt reduction to 1 – 5 nmol Fe L^{-1} at the shelf edge ~ 100 km offshore. A similar distribution pattern was observed for LP$_{Un}$Mn (Fig. 6(d)) and LP$_{Un}$Al (not shown), for cruises JR247 and JR274. Glacial melt has been reported as an important source of particulate material in the vicinity of the Antarctic Peninsula (de Jong et al., 2012). For example, Gerringa et al. (2012) documented elevated total dissolvable Fe concentration of up to 106 nmol L^{-1} near the Pine Island Glacier in the Amundsen Sea, and Raiswell et al. (2008) estimated that per year 1.6 Gmol nanoparticulate Fe, associated to ~~terrigenous~~ lithogenic particles, are delivered to the Southern Ocean by melting ice.

Locally elevated particulate metal concentrations in surface waters may also be related to production of faecal pellets by swarms of Antarctic krill (Schmidt et al., 2016). High abundances of Antarctic krill were estimated from acoustic backscattering observations

(Fielding et al., 2014), and large numbers of faecal pellets were observed on the SAPS filters during cruise JR247. The stomach content of Antarctic krill contained up to 90% sediment particles by volume, an observation that was attributed to filter feeding by these organisms on phytoplankton and seabed detritus, with incidental ingestion of deep ocean sediments (Schmidt et al., 2011) and glacial flour (Schmidt et al., 2016). Krill thus take up lithogenic (sediment) particles and transfer these into the surface ocean through the egestion of faecal pellets (Schmidt et al., 2016). The trace metal contents of krill faecal pellets collected during on-board incubation experiments during JR247 ranged from 0.88 – 67.14 μg Fe mg^{-1} dry weight (n = 27) (Table ~~4~~5) (Schmidt et al. 2016). The molar ratio PFe/PAl = 0.48 ± 0.07 and PMn/PAl = 0.0069 ± 0.001~~PFe/PMn = 70.5 ± 8.22~~ of the faecal pellets was similar to those for ~~suspended~~ sediment particles ~~in the water column~~ (~~PFe~~SFe/~~PMn~~ SAl = ~~68.0~~0.34 ± ~~0.6~~0.02 and PMn/PAl = 0.0066 ± 0.001; Table 1, 2, 3 and 4), indicating that Fe in krill faecal pellets was predominately associated with lithogenic (sediments) ~~terrigenous material~~ and/or glacial flour particles, as also reported by Schmidt et al. (2016). In contrast, the molar ratio PFe/~~PAl~~ PMn = 70.65~~0.48~~ ± ~~0.07~~8.22 of faecal pellets was ~~lower~~ higher than that of ~~suspended particles~~sediments, ~~PFe~~SFe/~~PAl~~ SMn = ~~1.25~~51.5 ± ~~0.0~~2.4, but just slightly higher than that of ~~sediments~~suspended SAPS particles, PFe/PAl = ~~0.34~~68.0 ± 0.~~02~~6. The observed variability in the PFe/PAl and PFe/PMn ratio in the various particle pools is therefore a consequence of ~~different contributions of biogenic material to the particulate reservoir and~~ different amounts of lithogenic and authigenic particles.~~Fe scavenged onto particle surfaces.~~

3.2 Supply routes of dissolved Fe, Mn, and Al

Concentrations of DFe, DMn, and DAl in the water column showed strong variations and ranged from ~ 0.1 – 25.9 nmol L^{-1}, 0.3 – 19.6 nmol L^{-1} and 0.1 – 18.4 nmol L^{-1}, respectively (Fig. 2, 5 and 7), with highest values in the surface waters in Cumberland Bay, and lowest beyond the shelf break (Fig. 6). Dissolved Fe concentrations from this study are in agreement with reported DFe near the Antarctic Peninsula (0.6 – 14.6 nmol L^{-1} (de Jong et al., 2012)) and Crozet Islands (0.1 – 2.5 nmol L^{-1} (Planquette et al., 2007)). Sources and sinks of dissolved trace metals, and their distribution in the water column are discussed in the following sections.

3.2.1 Supply from sediment pore waters

Elevated pore water concentrations of Fe and Mn (Fe_{PW} and Mn_{PW}) were observed in sediments from the southern shelf sites at water depths of around 250 m, and ranged from 0.5 – 110 µmol L^{-1} for Fe and 0.1 – 2 µmol L^{-1} for Mn (Fig. 7 and Table S2). The down-core distributions of Fe_{PW} and Mn_{PW} were consistent with microbial dissimilatory Mn and Fe reduction during organic matter oxidation (Canfield and Thamdrup, 2009), and thus concentrations were elevated at defined depth horizons controlled by their redox potential (Eh) (Bonneville et al., 2009; Raiswell and Canfield, 2012). The Fe_{PW} and Mn_{PW} concentrations near the sediment-seawater interface were used to calculate fluxes of Fe and Mn to bottom waters following diffusion of reduced Fe and Mn species across an oxygenated layer in surface sediments. These calculations were performed following Boudreau and Scott (1978) and Homoky et al. (2012), and are described in detailed in the Supplementary Text S3 and Table S1. We are aware that our calculated fluxes represent minimum estimates of pore water efflux, which under natural conditions is supplemented by advection due to bioirrigation, bioturbation, and bottom water currents (Homoky et al., 2016). In addition, sediment cores were collected on the southern shelf, while seawater and particulate samples were collected on the northern shelf side. The benthic Fe fluxes for the southern shelf maybe lower than those on the northern shelf, as an elevated primary productivity and enhanced particle export on the northern side will result in enhanced bacterial respiration, which reduces Eh and promotes the dissolution of Fe oxides with subsequent release of Fe into bottom waters.

Notwithstanding the above issues, we calculated substantial benthic fluxes from sediment pore waters to bottom waters on the southern shelf for Fe_{PW} of <0.1 to 44.4 µmol m^{-2} d^{-1} and Mn_{PW} of 0.6 to 4.1 µmol m^{-2} d^{-1}. The upper flux values for Fe are comparable to those reported for dysoxic and river-dominated continental margins (3.5 – 55 µmol m^{-2} d^{-1} (Homoky et al., 2012)), seasonal maxima of temperate and oxic shelf seas (23 – 31 µmol m^{-2} d^{-1} (Klar et al., 2017)), and shelf sediments off the Antarctic Peninsula (1.3 – 15.5 µmol m^{-2} d^{-1} (de Jong et al., 2012)). The Mn fluxes were relatively low for shelf environments, with for example fluxes of 70 – 4450 µmol m^{-2} d^{-1} reported for Baltic and Black Sea sediments (Pakhomova et al., 2007)). The Fe pore water fluxes from the South Georgia shelf sediments, which extend over an area of ca. 40,000 km^2, indicate that these may serve as an important year-round source to overlying waters, totalling 4 to 1,728 kmol DFe d^{-1} and 25 to 164 kmol DMn d^{-1}.

Benthic release of trace metal enriched pore waters shaped the distributions of dissolved trace metals in bottom waters on the shelf. Concentrations of DFe, DMn, and DAl were enhanced at isopycnals > 27.05 kg m^{-3} (e.g. DFe up to 7.70 nmol L^{-1} at site #21, Table 1) compared to surface waters (e.g. DFe as low as 0.30 nmol L^{-1} at site #13, Table 1; Fig. 2 and 7). Trace metal enriched bottom waters were also observed at sites #13, #14, #17 and #18 (Fig. 2). The molar DFe/DMn ratios in oxygenated bottom waters varied between 1.1 – 3.5 and were thus similar to pore waters near the sediment-seawater interface (0 – 1 cm depth, $Fe_{PW}/Mn_{PW} = 2.2 \pm 1.0$; Fig. 7). The similar trace metal ratios suggest that Fe and Mn in enriched pore waters crossed the sediment-bottom water interface and accumulated in shelf bottom waters.

To determine the vertical DFe fluxes from near bottom to surface waters we employed a method outlined by de Jong et al. (2012), and calculated both the advective and diffusive flux terms, which are not affected by the benthic Fe and Mn fluxes. We included the advective term in our calculations, because it has been shown that internal waves that cross shallow topographies and wind shear stress produces strong turbulence that facilitate Eckman upwelling (vertical advection) on the shelf (Kurapov et al., 2010; Moore, 2000; Wolanski and Delesalle, 1995). Applying literature values from the Southern Ocean for vertical diffusivity ($K_Z = 1 \times 10^{-4}$ m^2 s^{-1} (Charette et al., 2007)) and advective velocity ($w = 1.1 \times 10^{-6}$ m s^{-1} (de Jong et al., 2012)), an average vertical DFe flux on the shelf of 0.41 ± 0.26 µmol m^{-2} d^{-1} from subsurface waters into the surface mixed layer was estimated (Supplementary Text S4). The surface mixed layer depth was determined by a density criteria (~0.03 kg m^{-3} (de Boyer Montégut et al., 2004)) and was located at ~50 m depth. About 38% of the DFe flux was related to Ekman upwelling (advective term) and 62% to the diffusive flux. This vertical flux is at the lower end of the calculated benthic flux from this study (Fe_{PW} < 0.1 to 44.4 µmol m^{-2} d^{-1}), and agrees with values reported for other Southern Ocean shelf regions near the Antarctic Peninsula (within 20 – 70 km from the coast: ~ 2.7 ± 3.4 µmol m^{-2} d^{-1} (de Jong et al., 2012)) and the Crozet Islands (only diffusive flux of 0.06 µmol m^{-2} d^{-1} (Planquette et al., 2007)).

3.2.2 DFe supply from the leachable ~~particulate~~ fraction of particles

The analytical protocol for the analysis of SAPS-collected particulate material allows separate estimation of the refractory and leachable fractions of trace elements (R~~P~~ and L~~P~~, respectively). The R~~P~~ fraction of the suspended matter is considered to include silicates and aged oxide minerals, while the L~~P~~ fraction represents predominantly fresh oxyhydroxides, biogenic material and loosely bound surface associated elements which are readily remobilized using leaching procedures (Berger et al., 2008).

Concentrations of L~~P~~Fe, L~~P~~Mn and L~~P~~Al in the water column showed strong variations, ranging from a few picomoles to several nanomoles L^{-1} (Table 2). On average, L~~P~~Fe and L~~P~~Al concentrations at 150 m depth (~ 1.3 nmol L~~P~~Fe L^{-1} and ~0.95 nmol L~~P~~Al L^{-1}) were significantly higher than at 20 and 50 m, L~~P~~Fe = 0.3 nmol L^{-1} (student t-test: t[0.95;28] = 1.725 [1.703]; t[confidence level; n-1]); L~~P~~Al = 0.43 nmol L^{-1} (student t-test: t[0.90;28] = 1.383 [1.313]). The L~~P~~Mn concentrations did not vary strongly and remained near constant throughout the top 150 m (L~~P~~Mn = 8.9 pmol L^{-1} {student t-test: [0.65;28] = 0.400 [0.390]}). The average contribution of L~~P~~ to the particulate pool P~~,~~ (R~~P~~+L~~P~~), was low; 0.83 ± 1.13% for Fe, 2.55 ± 1.58% for Mn and 2.42 ± 1.32% for Al (Table 2). A study conducted in the North Pacific near the Columbia River outflow, reported considerably higher L~~P~~ fractions (e.g. 6.6±3.0% of Fe, 78.7±14.0% of Mn, 6.3±2.0% of Al (Berger et al., 2008)), which was attributed to enhanced biogenic particle levels in the low salinity waters of the river (Berger et al., 2008). In contrast, results from our study showed that particulate trace metals predominately had a refractory component (R~~P~~), indicating that Fe, Mn, and Al was mainly incorporated in ~~lithogenic material~~mineral structures unaffected by a weak leach (e.g. aged oxyhydroxides and alumosilicates).

A weak linear relationship between R~~P~~ and L~~P~~ was observed for Fe (R^2 = 0.57, n = 41), Mn (R^2 = 0.64, n = 41) and Al (R^2 = 0.63, n = 41) (Supplementary Fig. ~~S2~~ S3 and ~~S3~~S4), indicating that the L~~P~~ fraction included mainly lithogenic and authigenic (e.g. scavenged) Fe, Mn and Al ~~that was scavenged onto lithogenic particle surfaces~~ and not much L~~P~~Fe was incorporated in biogenic particles. The scavenging of dissolved trace metals by charged particle surfaces is established (Homoky et al., 2012; Koschinsky et al., 2003), but how well Fe and other trace metals can be remobilized from marine particle surfaces and which process may modify their availability over time is not yet well constrained (Achterberg et al., 2018; Fitzsimmons and Boyle, 2014; Milne et al., 2017).

For instance, scavenged Fe is reported to exchange with DFe in the water column of the tropical and high latitude North Atlantic (Achterberg et al., 2018; Fitzsimmons and Boyle, 2014; Milne et al., 2017). In addition, recent work has concluded that zooplankton grazing and the production of faecal pellets remobilizes DFe from lithogenic and biogenic particles (Giering et al., 2012; Schmidt et al., 2016). In contrast, freshly produced inorganic Fe(III) oxyhydroxide (FeOOH * nH_2O) precipitates in seawater are accessible but are subject to chemical and structural conversions that lead to less ~~soluble~~ leachable Fe with time (Yoshida et al., 2006).

3.2.3 DFe supply from Antarctic krill

Elevated dissolved trace metal concentrations in the top 200 m of the water column coincided with elevated particulate trace metal concentrations at sites #11/12, #15/16, #18, and #19/20 (Fig. 2, 5, and 7). The SAPS filters from these stations contained a high load of krill faecal pellets. To elucidate the relationship between dissolved trace metal concentrations and the local abundance of Antarctic krill and their faecal pellets, krill were caught and incubated on-board the vessel as described in Schmidt et al. (2016).

Antarctic krill excretion rates of DFe were variable, relating positively to the extent of recent ingestion of diatoms. However, on average krill released ~2.0 ± 1.9 nmol DFe individual^{-1} d^{-1} (Schmidt et al., 2016). By applying a mean krill abundance of 465 ± 588 individuals m^{-2}, estimated from acoustic backscattering measurements (Fielding et al., 2014), krill excreted 1.1 ± 2.2 µmol DFe m^{-2} d^{-1} into the top 300 m of the water column (Schmidt et al., 2016). In addition, krill produced ca. 1.8 ± 1.6 mg of faecal pellets per individual per day, containing ca. 0.30 ± 0.33 µmol Fe mg^{-1}. Particle leaches performed on those faecal pellet samples with 25% acetic acid showed that on average 2.5 ± 2.1% (9.3 ± 13.3 nmol Fe mg^{-1}) of the total Fe in these pellets could be remobilised (Table ~~4~~5), which would equate to a production of 14 ± 24 nmol L~~P~~Fe ind^{-1} d^{-1}. By multiplying the mean L~~P~~Fe by the ambient krill density used above, we calculate a L~~P~~Fe flux of 6.5 ± 8.2 µmol m^{-2} d^{-1} from the faecal pellets to the water column.

Since krill are mobile animals, questions remain over where the major part of the L~~P~~Fe flux occurs, and what the fate of this Fe source is. Highest krill abundances were recorded generally (but not exclusively) in the top 100 m layer (Fielding et al., 2014), and hence a large proportion of this L~~P~~Fe flux from krill is likely to occur in the upper waters. Notwithstanding our current uncertainties over the depths of origin and fate, the L~~P~~Fe flux from krill faecal pellets and the release of DFe were on average an order of magnitude higher than estimated vertical diffusive and advective DFe fluxes, with other grazers, such as copepods and salps, adding to the recycled flux estimates. This illustrates the importance of zooplankton-mediated-Fe-cycling, in agreement with previous studies (Hutchins and Bruland, 1994; Sato et al., 2007).

The experimental set-up did not allow us to establish the origin of the Fe released by krill, being both “recycled” Fe from biogenic material and “new” Fe from lithogenic (and authigenic) material. However, Schmidt et al. (2016) concluded that zooplankton gut passage mobilizes lithogenic Fe, and showed that there are strong spatial patterns in the organic and lithogenic make-up of faecal pellets. This included an exponential decline in the quantity of lithogenic particles in krill stomachs with distance from sources of glacial flour on the northern South Georgia coast. For instance, the lithogenic content at one site on the shelf contributed ~90% of stomach content volume suggesting that a large quantity of the accessible Fe was remobilized from those inorganic particles.

3.3 Off-shore transport of trace metal enriched water masses

Along a W – E transect (Fig. 1; #14 via # 13 to #11/12), lateral water mass transport carried suspended particles offshore. Because of the small size of the SAPS particulate data set (two data points), we considered the LP_{Un} fraction for this transect (Fig. 1). Indeed, elevated concentrations of the P and LP_{Un} metal fractions were observed in subsurface waters that had been in recent contact with the shelf. These metal-enriched waters, detected at the eastern shelf edge site #11/12 between 200 and 400 m water depth (Fig. 1 and 4), exhibited similar temperature and salinity signatures to shelf bottom waters. Furthermore, the elemental ratios of the LP_{Un} fraction in these waters were similar to the particles in the surface sediments (S1, S2, and S3) and the resuspended particles in the bottom boundary layer (#13 and #14) on the shallow shelf (Fig. 4). A similar distribution was also found for the P fractions, but limited to site #13 and #14, as SAPS were not deployed below 150 m at the shelf edge site #11/12.

The $LP_{Un}Fe$ concentration decreased with distance from the island to offshore: from site #14 at 200 m depth ($LP_{Un}Fe$ = 82.26 nmol L^{-1}; water depth = 255 m) to site #13 at 100 m depth ($LP_{Un}Fe$ = 34.06 nmol L^{-1}; water depth = 130 m) to site #11/12 between 200 and 400 m depth ($LP_{Un}Fe$ ~ 10.18 nmol L^{-1}; water depth = 750 m) (Fig.4 and Table 1). A similar decrease was observed for the SAPS Fe data: from site #14 at 150 m depth (PFe = 31.12 nmol L^{-1}) to site #13 at 100 m depth (PFe = 10.23 nmol L^{-1}). The decrease of PFe and $LP_{Un}Fe$ with increasing distance to the coast is in agreement with previous observations for the Western Subarctic Pacific (Lam and Bishop, 2008), which reported elevated L~~P~~Fe concentrations in the range of 0.6 to 3.8 nmol L^{-1} in subsurface waters between 100 and 200 m depth along the Kamchatka shelf and related this observation to offshore water mass transport. However, we assume that particles in the deep particulate Fe maximum are not transported over very large distances, due to their tendency to sink, and thus do not significantly contribute to the offshore Fe supply (section 3.4).

Consistent with the observed P and LP_{Un} distributions, elevated dissolved metal concentrations at depths between 200 and 400 m at site #11/12 indicated that trace metal enriched shelf bottom waters were transported offshore (Fig. 7). However, dissolved trace metal concentrations were more variable than P and LP_{Un}, and in case for DMn were highest at depths at shelf edge site #11/12. Notwithstanding the above issue, for horizontal flux calculations we used the entire DFe data set for water depths between 100 and 400 m. Average DFe concentrations in this depth range were highly variable and did not follow an exponential or power law function with distance from the coast (Supplementary Fig. ~~S4~~S5), which is necessary to determine scale length and horizontal diffusivity (K_h) (de Jong et al., 2012). As a result, horizontal flux calculations from the data could not be executed.

The distribution of dissolved trace metals in surface waters indicated that there was a limited transfer of DFe beyond the shelf break into the bloom region. Surface samples showed that DFe concentrations were strongly enriched in surface waters on the shelf (0.3 – 25.9 nmol L^{-1}, Fig. 6(b)), while DFe concentrations beyond the shelf break decreased abruptly to concentrations < 0.2 nmol L^{-1} (Fig. 6(b)). This indicates that DFe was quickly removed from ACC surface waters following passage of the island. However, previous studies in the region suggest DFe transfer beyond the shelf break of South Georgia (Borrione et al., 2013; Nielsdóttir et al., 2012). Nielsdóttir et al. (2012) reported surface waters downstream the island shelf with up to 2 nmol DFe L^{-1}, with seasonal variations and highest concentrations during austral summer in January/February 2008. Dissolved Fe data from JR247 (2011) and JR274 (2012) were also obtained during the summer season, but indicated rapid reduction in concentrations through mixing with DFe depleted ACC water, biological uptake and/or particle scavenging (authigenic precipitation).

3.4 Iron budget in the bloom region

Large seasonal phytoplankton blooms downstream of South Georgia recorded by earth observing satellites are initiated by Fe supplied by the South Georgia island/shelf system during the passage of ACC waters (Fig. 1) (Borrione et al., 2013; Nielsdóttir et al., 2012). Based on our study, the main DFe sources during this passage of the ACC were benthic release and vertical mixing, release of DFe from krill and krill faecal pellets, and supply of particles from run-off and glacial meltwater. In the following sections we will discuss the strength of each DFe source in the bloom region ca. 1,250 km downstream of the island and estimate how much DFe is required to stimulate the elevated primary productivity in that region. Because of the lack of observational data for the region, this part of the study combines literature values from different Southern Ocean studies. This approach contains large uncertainties that are discussed in detail in Section 3.4.6 Budget uncertainties.

3.4.1 Phytoplankton Fe requirements in the phytoplankton bloom region

The surface ocean in the vicinity of South Georgia during the austral summer features strongly elevated biomass production (Gilpin et al., 2002) and represents the largest known CO_2 sink in the ACC (12.9 mmol C m^{-2} d^{-1} (Jones et al., 2012)). The Fe requirements of the phytoplankton community in austral summer within the bloom that reaches several hundred kilometres downstream the island were determined by combining satellite-depth integrated net primary production data derived from a phytoplankton pigment adsorption (α_{ph})-based model (62 ± 21 mmol C m^{-2} d^{-1} (Ma et al., 2014)) over the period of 2003-2010 with an average intracellular Fe~~:~~/C ratio obtained from five Southern Ocean diatom species (5.23 ± 2.84 µmol Fe mol^{-1} C (Strzepek et al., 2011)). This approach yielded an approximate Fe requirement of 0.33 ± 0.11 µmol DFe m^{-2} d^{-1} for the phytoplankton community (Fig. 8). For a more detailed description of the applied values and calculations see Supplementary Text S4.

3.4.2 Horizontal and vertical mixing

De Jong et al. (2012) reported that horizontal and vertical advective, diffusive (diapycnal) and deep winter mixing downstream (1,250 – 1,570 km) of the Antarctic Peninsula (between 51°S and 59°S) supplied DFe to the surface waters in quantities that exceeded the DFe requirement of primary producers during austral summer (0.13 ± 0.04 µmol DFe m^{-2} d^{-1}). In their study region, de Jong et al. (2012) determined that ~ 0.30 ± 0.22 µmol DFe m^{-2} d^{-1} were supplied by horizontal and vertical fluxes, of which 91% of the vertical flux were attributed to Ekman upwelling (advective term), and 43% of the entire DFe flux was supplied by deep winter mixing. Tagliabue et al. (2014) reported similar model estimates for the region that is located south of the Polar Front and characterized by strong Ekman upwelling and winter entrainment.

For the bloom region downstream of South Georgia, model calculations by Tagliabue et al. (2014) indicated that less than 0.0003 µmol DFe m^{-2} d^{-1} were supplied by diapycnal mixing, and ~ -0.0027 µmol DFe m^{-2} d^{-1} were removed by Ekman down-welling. For the vertical flux component, this yields an overall loss of DFe of ~ -0.002 µmol DFe m^{-2} d^{-1} (0.0003 + (-0.0027)) in the bloom region north of South Georgia (Fig. 8).

Because the sampling in our study was not suitable for calculations of the horizontal flux, we applied the horizontal flux estimates from de Jong et al. (2012) for our own Fe budget. For a region ca. 1,250 km downstream of a source, calculations according to de Jong et al. (2012) sugest that ca. 0.11 ± 0.03 µmol DFe m^{-2} d^{-1} are supplied to the bloom region by horizontal advection and diffusion (Fig. 8).

3.4.3 Deep winter mixing

The entrainment of new DFe during winter represents an important Fe source to surface waters in the Southern Ocean (de Jong et al., 2012; Tagliabue et al., 2014). Elevated DFe concentrations in subsurface waters support primary production in the austral spring following entrainment by deep winter mixing. Model estimates showed that DFe supplied by winter mixing, together with diapycnal mixing, matches the Fe requirements at most low productivity sites in the Southern Ocean. However, deep winter mixing at the highly productive sites north of South Georgia supplies only ~ 0.011 µmol m^{-2} d^{-1} (Tagliabue et al., 2014) (Fig. 8). Later in the season primary productivity in surface waters is considered to rely strongly on Fe derived from recycling of biogenic material (Boyd et al., 2015).

3.4.4 Dust deposition

Dissolved Fe supplied by the deposition of aeolian dust is considered to be an important source to the Southern Ocean (Conway et al., 2015; Gabric et al., 2010; Gassó and Stein, 2007). Aeolian flux model estimates, supplied by Borrione et al. (2013) using a regional South Georgia model, suggested that up to 8 µmol Fe m^{-2} d^{-1} are delivered to the bloom regions downstream of South Georgia by dry and wet deposition. However, reliable dry and wet deposition estimates for the Southern Ocean are limited. Data from the South Atlantic along 40°S, ~ 1.000 km north of South Georgia, showed that rather low levels of DFe (~ 0.002 µmol m^{-2} d^{-1}) are supplied by dry deposition (Chance et al., 2015). In addition, ~ 1.0 ± 1.2 µmol DFe m^{-2} d^{-1} are delivered sporadically to the 40°S area by wet deposition (Chance et al., 2015). However, even when assuming that similar wet deposition fluxes occur north of South Georgia, fertilization with DFe is temporally and spatially limited. Furthermore, it is very unlikely that such sporadic events could cause long-lasting and far extending phytoplankton blooms strictly constrained between the PF and the SACCF.

3.4.5 Luxury Fe uptake on the shelf

Our conservative estimate of DFe supply to the bloom region by vertical/horizontal mixing, deep winter entrainment and dust deposition (< 0.12 µmol Fe m^{-2} d^{-1}) covers only ~30% of the estimated phytoplankton requirements (~ 0.33 µmol Fe m^{-2} d^{-1}) (Fig. 8). We hypothesize that the missing supply of ~ 0.21 µmol DFe m^{-2} d^{-1} is supplied to the bloom region through the off-shore advection of phytoplankton cells that are enriched in labile Fe. It has been demonstrated that Fe-rich biogenic particles can be created by luxury iron uptake of diatoms (Iwade et al., 2006; Marchetti et al., 2009). Using bottle incubation experiments, Iwade et al. (2006) showed that under Fe replete conditions the coastal diatom *Chaetoceros sociale* stores more intracellular Fe than needed for the production of essential enzymes and proteins. We therefore hypothesize that phytoplankton cells that grew under excess nutrient supply on the South Georgia shelf stored more Fe than needed for their metabolic processes. Due to subsequent cycles of grazing, lysis or bacterial decomposition, this iron can be remobilised in surface waters and made available for renewed phytoplankton uptake.

High Fe recycling efficiencies, described by the f*e* ratio (Boyd et al., 2005), are required to maintain the cycle of remineralisation and uptake in the euphotic zone. This counteracts the loss of particulate Fe by vertical export. Boyd et al. (2015) reported the highest recycling efficiencies of ~ 90% for subantarctic, DFe-deplete waters such as downstream of South Georgia. Further, these workers showed that the degree of recycling is controlled by the abundance of prokaryotes with a high Fe quota, such as cyanobacteria, and particularly by grazing zooplankton. The waters off South Georgia feature among the highest biomasses worldwide of metazoan grazers (Atkinson et al., 2001). These large grazers, chiefly copepods and Antarctic krill, are able to efficiently ingest large diatoms including species that are known to store luxury iron (Atkinson, 1994; Hamm et al., 2003), thereby disintegrating cell membranes and releasing trace metals.

In recent years it has become apparent that the recycling of biogenic particles in the euphotic zone is a critical mechanism that maintains primary production, especially when the dissolved nutrient pools become exhausted (Boyd et al., 2015; Tagliabue et al., 2014). However, uncertainties remain over the degree to which Fe is lost during each cycle of uptake and remineralisation. Thus more research is needed, especially field work that encompasses the community structures (bacteria, phytoplankton, zooplankton, and higher predators (Ratnarajah et al., 2017; Wing et al., 2014)), the degree of recycling for macro- and micro-nutrients in the euphotic zone, and loss of Fe through vertical export.

An alternative explanation to our suggestion that recycling of luxury iron enriched biota contributes to the downstream bloom is that iron is adsorbed directly onto particles that are advected directly offshore. For example freshly precipitated Fe(III) oxyhydroxides (FeOOH * nH_2O) may be adsorbed onto biogenic and non-biogenic material. Iron freshly absorbed onto biogenic and non-biogenic material can be released and incorporated by phytoplankton and bacteria. However, the bioavailability of adsorbed and inorganic Fe changes over time. Both Wells et al. (1991) and Chen and Wang (2001) demonstrated that the bioavailability of freshly precipitated FeOOH and Fe adsorbed onto colloids/inorganic particles decreases over time. This is primarily due to the dehydration of the loosely packed structure that is subsequently transferred into amorphous FeOOH in the mineral structure Goethite. Because of this we suggest that the majority of Fe from inorganic FeOOH or Fe adsorbed onto particles must be released and utilized in an early stage of the voyage, mainly on the shelf or shortly after the shelf break.

3.4.6 Budget uncertainties

Estimates for Fe budgets are challenging and often contain large uncertainties. This is primarily due to the lack of site- and time-specific flux data. Moreover, the mean annual estimates, necessary for reliable supply calculations, reach a high level of accuracy only after the same region has been monitored multiple times to cover seasonal and annual anomalies. In the following, we will discuss the uncertainty of the different Fe fluxes in the blooming region north of South Georgia.

We identified three main processes that account together for ~98% of the total Fe flux in the blooming region, and thus contribute largest uncertainties; the horizontal flux, dry/wet deposition, and winter entrainment. Horizontal flux estimates of this study rely on literature values that were collected offshore the Antarctic Peninsula. In contrast, South Georgia is an island with a confined shelf region and thus horizontal DFe fluxes may differ greatly. Furthermore, we showed that dry deposition dust fluxes are generally low, but showed in addition that the Fe flux can be supplemented strongly by sporadic wet deposition events (~ 1.0 ± 1.2 µmol DFe m^{-2} d^{-1}) (Chance et al., 2015). Atmospheric fluxes are variable, illustrated by the large standard deviation of the wet deposition Fe fluxes obtained at 40°S. Furthermore, to determine the magnitude of the seasonal DFe winter entrainment reliable estimates of the winter mixing layer depth (WMLD) and the ferrocline are required. Even though the WMLD can be estimated very precisely using Argo float data, the depth of ferrocline in the manuscript of Tagliabue et al. (2014) is based on 140 unique observations distributed over the entire Southern Ocean. Due to this regional anomalies are not captured. In addition to the DFe fluxes in the blooming region, we also assume that the biological Fe demand estimated for the phytoplankton community contributes a large error. The biological Fe requirements were determined using satellite derived net primary production data and an average intracellular Fe~~:~~/C ratio derived from 5 different diatom species native to the Southern Ocean. Both parameters are not well constrained and because of the lack of observational data we applied the lowest intracellular Fe~~:~~/C ratio available in the literature (Strzepek et al., 2011). However, we found that even small changes of the both parameters change the estimated Fe availability in the bloom region strongly. Nevertheless, flux estimates even with large uncertainties can help us understand the degree of the nutrient supply vs. consumption by organisms and help to pinpoint the limitation of the estimates made. To ultimately reduce the level of uncertainty and to improve our biogeochemical models more observational data from the bloom region north of South Georgia is required.

4. Conclusions

Shelf sediment-derived Fe and Fe released from Antarctic krill significantly contribute to the DFe distribution in the shelf waters around South Georgia. Nevertheless, DFe enriched in shelf waters are not effectively advected to the phytoplankton bloom region downstream of the island. Together with other Fe supplies, such as aeolian dust, deep winter mixing and diapycnal mixing, the horizontal advection contributes only ~30% to the Fe requirements of a phytoplankton bloom downstream of South Georgia. We therefore hypothesize that the majority of the Fe is derived from remineralisation of Fe enriched phytoplankton cells and biogenic particles that are transported with the water masses into the bloom region.

While we highlight the importance of grazers and the cycling of various particulate Fe phases in the Fe-fertilisation of the South Georgia bloom, more work is needed to clarify the transport mechanisms of dissolved and particulate Fe.

Author contribution

CS, KS, EPA, SF, and AAt designed the experiments for JC247. CS, MDP and AAt performed the sampling and krill incubation experiments during JC247. CS and MC analysed the trace metal samples at NOCS. EPA sampled the seawater during JC274. Samples from JC274 were analysed by CS and MC. AAq, WBH and RM designed the experiments for JR55 and AAq analysed the samples. CS prepared the manuscript with contributions from all co-authors.

Acknowledgements

We would like to thank the officers and crew of RRS *James Clark Ross* for assistance with the pelagic sampling and those of RRS *James Cook* for the benthic coring. In addition, we thank the two anonymous reviewers for reviewing the manuscript. This work forms part of the NERC-AFI grant AFI9/07 to AA and EA (NE/F01547X/1). RAM was funded by NERC grants NE/01249X/1 and NE/H004394/1. WBH was supported by NERC fellowship NE/K009532/1

References

Achterberg, E. P., Steigenberger, S., Marsay, C. M., LeMoigne, F. A. C., Painter, S. C., Baker, A. R., Connelly, D. P., Moore, C. M., Tagliabue, A., and Tanhua, T.: Iron Biogeochemistry in the High Latitude North Atlantic Ocean, Scientific Reports, 8,-1283, 2018.

Atkinson, A.: Diets and feeding selectivity among the epipelagic copepod community near South Georgia in summer, Polar Biol., 14, 551-560, 1994.

Atkinson, A., Whitehouse, M. J., Priddle, J., Cripps, G. C., Ward, P., and Brandon, M. A.: South Georgia, Antarctica: a productive, cold water, pelagic ecosystem, Mar. Ecol.-Prog. Ser., 216, 279-308, 2001.

Berger, C. J. M., Lippiatt, S. M., Lawrence, M. G., and Bruland, K. W.: Application of a chemical leach technique for estimating labile particulate aluminum, iron, and manganese in the Columbia River plume and coastal waters off Oregon and Washington, J. Geophys. Res., 113, 1-16, 2008.

Bonneville, S., Behrends, T., and Van Cappellen, P.: Solubility and dissimilatory reduction kinetics of iron(III) oxyhydroxides: A linear free energy relationship, Geochim. Cosmochim. Act., 73, 5273-5282, 2009.

Borrione, I., Aumont, O., Nielsdottir, M. C., and Schlitzer, R.: Sedimentary and atmospheric sources of iron around South Georgia, Southern Ocean: a modelling perspective, Biogeosciences Discuss., 10, 10811-10858, 2013.

Boudreau, B. P. and Scott, M. R.: A model for the diffusion-controlled growth of deep-sea manganese nodules, Americ. J. Sc., 278, 903-929, 1978.

Boyd, P. W., Law, C. S., Hutchins, D. A., Abraham, E. R., Croot, P. L., Ellwood, M., Frew, R. D., Hadfield, M., Hall, J., Handy, S., Hare, C., Higgins, J., Hill, P., Hunter, K. A., LeBlanc, K., Maldonado, M. T., McKay, R. M., Mioni, C., Oliver, M., Pickmere, S., Pinkerton, M., Safi, K., Sander, S., Sanudo-Wilhelmy, S. A., Smith, M., Strzepek, R., Tovar-Sanchez, A., and Wilhelm, S. W.: FeCycle: Attempting an iron biogeochemical budget from a mesoscale SF6 tracer experiment in unperturbed low iron waters, Global Biogeochem. Cycles, 19, 1-13, 2005.

Boyd, P. W., Strzepek, R. F., Ellwood, M. J., Hutchins, D. A., Nodder, S. D., Twining, B. S., and Wilhelm, S. W.: Why are biotic iron pools uniform across high- and low-iron pelagic ecosystems?, Global Biogeochem. Cycles, 29, 1028-1043, 2015.

Browning, T. J., Bouman, H. A., Henderson, G. M., Mather, T. A., Pyle, D. M., Schlosser, C., Woodward, E. M. S., and Moore, C. M.: Strong responses of Southern Ocean phytoplankton communities to volcanic ash, Geophys. Res. Lett., 41, 1-7, 2014.

Buesseler, K. O., Andrews, J. E., Pike, S. M., and Charette, M. A.: The Effects of Iron Fertilization on Carbon Sequestration in the Southern Ocean, Science, 304, 414-417, 2004.

Canfield, D. E. and Thamdrup, B.: Towards a consistent classification scheme for geochemical environments, or, why we wish the term ‘suboxic’ would go away, Geobiol., 7, 385-392, 2009.

Cassar, N., Bender, M. L., Barnett, B. A., Fan, S., Moxim, W. J., Levy II, H., and Tilbrook, B.: The Southern Ocean Biological Response to Aelian Iron Input, Science, 317, 1067-1070, 2007.

Chance, R., Jickells, T. D., and Baker, A. R.: Atmospheric trace metal concentrations, solubility and deposition fluxes in remote marine air over the south-east Atlantic, Mar. Chem., 177, 45-55, 2015.

Charette, M. A., Gonneea, M. E., Morris, P., Statham, P., Fones, G., Planquette, H., Salter, I., and Garabato, A. N.: Radium isotopes as tracers of iron sources fueling a Southern Ocean phytoplankton bloom, Deep-Sea Res. II, 54, 1989-1998, 2007.

Chase, Z., Hales, B., Cowles, T., Schwartz, R., and van Geen, A.: Distribution and variability of iron input to Oregon coastal waters during the upwelling season, J. Geophys. Res., 110, 1-14, 2005.

Chen, M. and Wang, W.-X.: Bioavailability of natural colloid-bound iron to marine plankton: Influences of colloidal size and aging, Limnol. Oceanogr., 46, 1956-1967, 2001.

Conway, T. M., Wolff, E. W., Rothlisberger, R., Mulvaney, R., and Elderfield, H. E.: Constraints on soluble aerosol iron flux to the Southern Ocean at the Last Glacial Maximum, Nat. Commun., 6, 1-9, 2015.

de Boyer Montégut, C., Madec, G., Fischer, A. S., Lazar, A., and Iudicone, D.: Mixed layer depth over the global ocean: An examination of profile data and a profile-based climatology, J. Geophys. Res., 109, 1-20, 2004.

de Jong, J., Schoemann, V., Lannuzel, D., Croot, P., de Baar, H. J. W., and Tison, J. L.: Natural iron fertilization of the Atlantic sector of the Southern Ocean by continental shelf sources of the Antarctic Peninsula, J. Geophys. Res., 117, 1-25, 2012.

Fielding, S., Watkins, J. L., Trathan, P. N., Enderlein, P., Waluda, C. M., Stowasser, G., Tarling, G. A., and Murphy, E. J.: Interannual variability in Antarctic krill (Euphausia superba) density at South Georgia, Southern Ocean: 1997–2013, ICES J. Mar. Sci., 2014. 1-11, 2014.

Fitzsimmons, J. N. and Boyle, E. A.: Both soluble and colloidal iron phases control dissolved iron variability in the tropical North Atlantic Ocean, Geochim. Cosmochim. Act., 125, 539-550, 2014.

Gabric, A. J., Cropp, R. A., McTainsh, G. H., Johnston, B. M., Butler, H., Tilbrook, B., and Keywood, M.: Australian dust storms in 2002 and 2003 and their impact on Southern Ocean biogeochemistry, Global Biogeochem. Cycles, 24, 1-17, 2010.

Gao, Y., Kaufman, Y. J., Tanré, D., Kolber, D., and Falkowski, P. G.: Seasonal distributions of aeolian iron fluxes to the global ocean, Geophys. Res. Lett., 28, 29-32, 2001.

Gassó, S. and Stein, A. F.: Does dust from Patagonia reach the sub-Antarctic Atlantic Ocean?, Geophys. Res. Lett., 34, 1-5, 2007.

German, C. R., Casciotti, K. A., Dutay, J.-C., Heimbürger, L. E., Jenkins, W. J., Measures, C. I., Mills, R. A., Obata, H., Schlitzer, R., Tagliabue, A., Turner, D. R., and Whitby, H.: Hydrothermal impacts on trace element and isotope ocean biogeochemistry, Philos Trans A Math Phys Eng Sci, 374, 1-19, 2016.

Gerringa, L. J. A., Alderkamp, A.-C., Laan, P., Thuróczy, C.-E., De Baar, H. J. W., Mills, M. M., van Dijken, G. L., van Haren, H., and Arrigo, K. R.: Iron from melting glaciers fuels the phytoplankton blooms in Amundsen Sea (Southern Ocean): Iron biogeochemistry, Deep-Sea Res. II, 71-76, 16-31, 2012.

Giering, S. L. C., Steigenberger, S., Achterberg, E. P., Sanders, R., and Mayor, D. J.: Elevated iron to nitrogen recycling by mesozooplankton in the Northeast Atlantic Ocean, Geophys. Res. Lett., 39, L12608, 2012.

Gilpin, L. C., Priddle, J., Whitehouse, M. J., Savidge, G., and Atkinson, A.: Primary production and carbon uptake dynamics in the vicinity of South Georgia-balancing carbon fixation and removal, Mar. Ecol. Prog. Ser., 242, 51-62, 2002.

Hamm, C. E., Merkel, R., Springer, O., Jurkojc, P., Maier, C., Prechtel, K., and Smetacek, V.: Architecture and material properties of diatom shells provide effective mechanical protection, Nature, 421, 841-843, 2003.

Ho, T.-Y., Quigg, A., Finkel, Z. V., Milligan, A. J., Wyman, K., Falkowski, P. G., and Morel, F. M. M.: The elemental composition of some marine phytoplankton, J. Phycol., 39, 1145-1159, 2003.

Homoky, W. B., Hembury, D. J., Hepburn, L. E., Mills, R. A., Statham, P. J., Fones, G. R., and Palmer, M. R.: Iron and manganese diagenesis in deep sea volcanogenic sediments and the origins of pore water colloids, Geochim. Cosmochim. Act., 75, 5032-5048, 2011.

Homoky, W. B., Severmann, S., McManus, J., Berelson, W. M., Riedel, T. E., Statham, P. J., and Mills, R. A.: Dissolved oxygen and suspended particles regulate the benthic flux of iron from continental margins, Mar. Chem., 134–135, 59-70, 2012.

Homoky, W. B., Weber, T., Berelson, W. M., Conway, T. M., Henderson, G. M., van Hulten, M., Jeandel, C., Severmann, S., and Tagliabue, A.: Quantifying trace element and isotope fluxes at the ocean–sediment boundary: a review, Philos Trans A Math Phys Eng Sci, 374, 2016.

Hutchins, D. A. and Bruland, K. W.: Grazer-mediated regeneration and assimilation of Fe, Zn and Mn from planktonic prey, Mar. Ecol.-Prog. Ser., 110, 259-269, 1994.

Iwade, S., Kuma, K., Isoda, Y., Yoshida, M., Kudo, I., Nishioka, J., and Suzuki, K.: Effect of high iron concentrations on iron uptake and growth of a coastal diatom Chaetoceros sociale, Aquat. Microb. Ecol., 43, 177-191, 2006.

Jones, E. M., Bakker, D. C. E., Venables, H. J., and Hardman-Mountford, N. J.: Seasonal cycle of CO2 from the sea ice edge to island blooms in the Scotia Sea, Southern Ocean, Mar. Chem., 177, 490-500, 2015.

Jones, E. M., Bakker, D. C. E., Venables, H. J., and Watson, A. J.: Dynamic seasonal cycling of inorganic carbon downstream of South Georgia, Southern Ocean, Deep-Sea Res. II, 59–60, 25-35, 2012.

Kalnejais, L. H., Martin, W. R., and Bothner, M. H.: The release of dissolved nutrients and metals from coastal sediments due to resuspension, Mar. Chem., 121, 224-235, 2010.

Klar, J. K., Homoky, W. B., Statham, P. J., Birchill, A. J., Harris, E. L., Woodward, E. M. S., Silburn, B., Cooper, M. J., James, R. H., Connelly, D. P., Chever, F., Lichtschlag, A., and

Graves, C.: Stability of dissolved and soluble Fe(II) in shelf sediment pore waters and release to an oxic water column, Biogeochemistry, 2017. 1-19, 2017.

Korb, R. E., Whitehouse, M. J., and Ward, P.: SeaWiFS in the southern ocean: spatial and temporal variability in phytoplankton biomass around South Georgia, Deep-Sea Res. II, 51, 99-116, 2004.

Koschinsky, A., Winkler, A., and Fritsche, U.: Importance of different types of marine particles for the scavenging of heavy metals in the deep-sea bottom water, Appl Geochem, 18, 693-710, 2003.

Kurapov, A. L., Allen, J. S., and Egbert, G. D.: Combined Effects of Wind-Driven Upwelling and Internal Tide on the Continental Shelf, Journal of Physical Oceanography, 40, 737-756, 2010.

Lam, P. J. and Bishop, J. K. B.: The continental margin is a key source of iron to the HNLC North Pacific Ocean, Geophys. Res. Lett., 35, 1-5, 2008.

Liu, X. and Millero, F. J.: The solubility of iron in seawater, Mar. Chem., 77, 43-54, 2002.

Ma, S., Tao, Z., Yang, X., Yu, Y., Zhou, X., M, W., and Li, Z.: Estimation of marine primary productivity from satellite-derived phytoplankton absorption data, IEEE J-STARS, 7, 3084-3092, 2014.

Marchetti, A., Parker, M. S., Moccia, L. P., Lin, E. O., Arrieta, A. L., Ribalet, F., Murphy, M. E. P., Maldonado, M. T., and Armbrust, E. V.: Ferritin is used for iron storage in bloom-forming marine pennate diatoms, Nature, 457, 467-470, 2009.

Marsay, C. M., Sedwick, P. N., Dinniman, M. S., Barrett, P. M., Mack, S. L., and McGillicuddy, D. J.: Estimating the benthic efflux of dissolved iron on the Ross Sea continental shelf, Geophys. Res. Lett., 41, 7576-7583, 2014.

Meredith, M. P., Brandon, M. A., Murphy, E. J., Trathan, P. N., Thorpe, S. E., Bone, D. G., Chernyshkov, P. P., and Sushin, V. A.: Variability in hydrographic conditions to the east and northwest of South Georgia, 1996–2001, J. Marine Syst., 53, 143-167, 2005.

Milne, A., Schlosser, C., Wake, B. D., Achterberg, E. P., Chance, R., Baker, A. R., Forryan, A., and Lohan, M. C.: Particulate phases are key in controlling dissolved iron concentrations in the (sub)tropical North Atlantic, Geophys. Res. Lett., 44, 2377-2387, 2017.

Moore, W. S.: Determining coastal mixing rates using radium isotopes, Cont. Shelf Res., 20, 1993-2007, 2000.

Murphy, E. J., Trathan, P. N., Watkins, J. L., Reid, K., Meredith, M. P., Forcada, J., Thorpe, S. E., Johnston, N. M., and Rothery, P.: Climatically driven fluctuations in Southern Ocean ecosystems, P ROY SOC B-BIOL SCI, 274, 3057-3067, 2007.

Nielsdóttir, M. C., Bibby, T. S., Moore, C. M., Hinz, D. J., Sanders, R., Whitehouse, M., Korb, R., and Achterberg, E. P.: Seasonal and spatial dynamics of iron availability in the Scotia Sea, Mar. Chem., 130–131, 62-72, 2012.

Pakhomova, S. V., Hall, P. O. J., Kononets, M. Y., Rozanov, A. G., Tengberg, A., and Vershinin, A. V.: Fluxes of iron and manganese across the sediment–water interface under various redox conditions, Mar. Chem., 107, 319-331, 2007.

Planquette, H., Sanders, R., Statham, P. J., Morris, P. J., and Fones, G. R.: Fluxes of particulate iron from the upper ocean around the Crozet Islands: A naturally iron-fertilized environment in the Southern Ocean, Global Biogeochem. Cycles, 25, 1-12, 2011.

Planquette, H., Statham, P. J., Fones, G. R., Charette, M. A., Moore, C. M., Salter, I., Nedelec, F. H., Taylor, S. L., French, M., Baker, A. R., Mahowald, N., and Jickells, T. D.: Dissolved iron in the vicinity of the Crozet Islands, Southern Ocean, Deep-Sea Res. II, 54, 1999-2019, 2007.

Pollard, R. T., Salter, I., Sanders, R. J., Lucas, M. I., Moore, C. M., Mills, R. A., Statham, P. J., Allen, J. T., Baker, A. R., Bakker, D. C. E., Charette, M. A., Fielding, S., Fones, G. R., French, M., Hickman, A. E., Holland, R. J., Hughes, J. A., Jickells, T. D., Lampitt, R. S., Morris, P. J., Nedelec, F. H., Nielsdottir, M., Planquette, H., Popova, E. E., Poulton, A. J., Read, J. F., Seeyave, S., Smith, T., Stinchcombe, M., Taylor, S., Thomalla, S., Venables, H. J., Williamson, R., and Zubkov, M. V.: Southern Ocean deep-water carbon export enhanced by natural iron fertilization, Nature, 457, 577-580, 2009.

Raiswell, R., Benning, L. G., Tranter, M., and Tulaczyk, S.: Bioavailable iron in the Southern Ocean: the significance of the iceberg conveyor belt, Geochemical Transactions, 9, 1-9, 2008.

Raiswell, R. and Canfield, D. E.: The Iron Biogeochemical Cycle Past and Present, Geochemical Perspectives, 1, 1-2, 2012.

Rapp, I., Schlosser, C., Rusiecka, D., Gledhill, M., and Achterberg, E. P.: Automated preconcentration of Fe, Zn, Cu, Ni, Cd, Pb, Co, and Mn in seawater with analysis using high-resolution sector field inductively-coupled plasma mass spectrometry, Anal. Chimi. Acta, 976, 1-13, 2017.

Ratnarajah, L., Lannuzel, D., Townsend, A. T., Meiners, K. M., Nicol, S., Friedlaender, A. S., and Bowie, A. R.: Physical speciation and solubility of iron from baleen whale faecal material, Mar. Chem., 2017. 2017.

Sato, M., Takeda, S., and Furuya, K.: Iron regeneration and organic iron(III)-binding ligand production during in situ zooplankton grazing experiment, Mar. Chem., 106, 471-488, 2007.

Schlosser, C., De La Rocha, C. L., and Croot, P. L.: Effects of iron surface adsorption and sample handling on iron solubility measurements, Mar. Chem., 127, 48-55, 2011.

Schmidt, K., Atkinson, A., Steigenberger, S., Fielding, S., Lindsay, M. C. M., Pond, D. W., Tarling, G. A., Klevjer, T. A., Allen, C. S., Nicol, S., and Achterberg, E. P.: Seabed foreaging by Antarctic krill: Implications for stock assessment, bentho-pelagic coupling, and the vertical transfer of iron, Limnol. Oceanogr., 56, 1411-1428, 2011.

Schmidt, K., Schlosser, C., Atkinson, A., Fielding, S., Venables, H. J., Waluda, C. M., and Achterberg, E. P.: Zooplankton gut passage mobilises lithogenic iron for ocean productivity, Curr. Biol., 26, 1-7, 2016.

Strzepek, R., Maldonado, M. T., Hunter, K. A., Frew, R. D., and Boyd, P. W.: Adaptive strategies by Southern Ocean phytoplankton to lessen iron limitation: Uptake of organically complexed iron and reduced cellular iron requirements, Limnol. Oceanogr., 56, 1983-2002, 2011.

Tagliabue, A., Sallee, J.-B., Bowie, A. R., Levy, M., Swart, S., and Boyd, P. W.: Surface-water iron supplies in the Southern Ocean sustained by deep winter mixing, Nat Geosci, 7, 314-320, 2014.

Tsuda, A., Saito, H., Machida, R. J., and Shimode, S.: Meso- and microzooplankton responses to an in situ iron fertilization experiment (SEEDS II) in the northwest subarctic Pacific, Deep-Sea Res. II, 56, 2767-2778, 2009.

Wedepohl, K. H.: The composition of the continental crust, Geochim. Cosmochim. Act., 59, 1217-1232, 1995.

Wells, M. L., Mayer, L. M., Donard, O. F. X., Sierra, M. M. D., and Ackelson, S. G.: The Photolysis Of Colloidal Iron In The Oceans, Nature, 353, 248-250, 1991.

Whitehouse, M. J., Korb, R. E., Atkinson, A., Thorpe, S. E., and Gordon, M.: Formation, transport and decay of an intense phytoplankton bloom within the High-Nutrient Low-Chlorophyll belt of the Southern Ocean, J. Marine Syst., 70, 150-167, 2008.

Wing, S. R., Jack, L., Shatova, O., Leichter, J. J., Barr, D., Frew R. D., and Gault-Ringold, M.: Seabirds and marine mammals redistribute bioavailable iron in the Southern Ocean, Mar. Ecol. Prog. Ser., 510, 1-13, 2014.

Wolanski, E. J. and Delesalle, B.: Upwelling by internal waves, Tahiti, French Polynesia, Cont. Shelf Res., 15, 357-368, 1995.

Yoshida, M., Kuma, K., Iwade, S., Isoda, Y., Takata, H., and Yamada, M.: Effect of aging time on the availability of freshly precipitated ferric hydroxide to costal marine diatoms, Mar. Biol., 149, 379-392, 2006.

Table 1: OTE-seawater samples: Fe, Mn, and Al concentrations determined for the dissolved (D) (0.2 µm) and the leachable particulate fraction (LP_{UN}) (total dissolvable – dissolved) of unfiltered seawater samples collected during JR247. Additional information covers sampling date, site (station) ID, event number and latitude + longitude.

Date	Site ID	Depth	Leach. Part. (nmol L^{-1})			Dissolved (nmol L^{-1})		
	Lat. & Lon.	(m)	LP_{Un}Fe	LP_{Un}Mn	LP_{Un}Al	DFe	DMn	DAl
04/01/2011	#9/10 (E95 & E97)	20	20.36	0.95	46.41	5.71	1.83	1.11
		50	15.18	0.42	40.86	3.19	1.88	2.27
	54.26°S, 35.35°W	100	9.86	0.23	20.43	1.55	0.92	2.07
		130	23.33	0.73	48.91	2.82	0.87	2.68
		150	23.71	0.43	46.95	2.35	1.03	0.12
		200	27.37	0.62	54.41	2.70	0.89	2.37
05/01/2011	#11/12 (E98 & E101)	20	4.05	0.38	6.68	2.19	0.41	3.57
		35	1.52	0.39	7.28	0.41	0.37	-
	54.62°S, 34.81°W	50	9.30	0.60	22.20	7.18	0.64	13.31
		75	1.28	0.31	7.85	0.77	0.35	4.56
		100	2.02	0.32	3.34	1.09	0.35	1.47
		150	1.55	0.38	3.18	1.10	0.45	-
		200	13.10	1.31	23.81	1.26	1.17	3.07
		300	8.62	0.70	23.25	1.06	0.55	-
		400	8.81	0.54	16.54	2.05	0.46	2.69
		500	4.51	0.41	11.41	0.72	0.38	0.76
		600	2.75	0.37	10.32	0.96	0.36	0.77
		700	4.81	0.41	16.85	0.82	0.35	-
06/01/2011	#13 (E105)	20	3.46	0.62	14.68	0.28	0.57	4.53
		35	1.00	0.33	7.17	0.10	0.28	2.64
	54.53°S, 35.27°W	50	7.09	0.71	22.62	1.26	0.57	5.77
		75	25.03	1.09	61.94	1.23	0.64	5.86
		100	34.06	1.30	87.43	0.82	0.74	4.08
07/01/2011	#14 (E113)	20	4.00	0.89	7.87	0.64	0.85	2.57
		50	2.23	0.31	7.64	0.27	0.32	1.80
	54.56°S, 35.59°W	75	2.30	0.43	3.58	0.62	0.46	2.42
		100	2.26	0.44	3.34	0.35	0.46	0.46
		150	23.50	0.94	33.35	0.70	0.62	0.23
		200	82.26	2.12	103.11	2.69	0.77	2.31
08/01/2011	#15/16 (E119 & E129)	20	17.66	0.46	26.66	0.99	1.36	-
		35	16.60	0.30	13.37	0.96	1.27	-
	53.62°S, 36.34°W	50	16.30	0.23	18.49	1.21	1.40	-
		75	23.82	0.56	29.86	0.98	1.28	-
		100	8.49	0.10	10.50	0.73	0.56	-
		150	1.88	0.03	4.49	2.25	0.40	-
		200	2.72	0.02	1.40	0.63	0.44	2.87

		300	2.56	0.05	2.40	0.34	0.25	-
		400	3.75	0.02	5.28	0.48	0.30	1.17
		500	5.28	0.08	9.22	0.43	0.30	-
		600	5.50	0.09	11.45	0.53	0.28	1.63
		750	5.27	0.06	8.16	0.44	0.30	-
10/01/2011	#17 (E133)	20	10.92	0.22	7.43	2.31	1.20	3.76
		35	20.83	0.53	16.22	1.81	1.34	2.56
	53.90°S, 36.57°W	50	34.59	1.00	57.55	2.29	1.42	2.33
		75	118.25	2.18	64.36	4.21	1.86	2.19
		100	50.71	1.00	77.52	2.48	1.42	1.62
		150	112.28	2.23	86.09	3.39	1.41	0.86
11/01/2011	#18 (E138)	20	106.71	1.77	95.17	2.75	1.57	3.36
		35	83.53	0.00	100.32	1.97	1.33	2.44
	54.10°S, 36.25°W	50	9.67	0.00	18.23	0.74	0.85	-
		75	5.65	0.00	8.90	0.62	0.65	-
		100	4.50	0.08	23.65	1.25	0.48	5.18
		150	7.81	0.11	12.87	1.43	0.49	8.19
12/01/2011	#19/20 (E141 & E143)	20	60.19	2.11	54.29	1.46	1.71	5.30
		35	60.17	2.19	87.17	1.34	1.90	8.22
	53.54°S, 38.11°W	50	66.78	2.74	141.75	1.57	1.90	8.73
		75	71.69	1.78	79.19	1.61	2.13	11.45
		100	10.77	0.25	32.12	0.99	0.67	10.74
		150	5.43	0.13	31.35	1.84	0.92	12.00
		200	7.92	0.14	27.42	1.45	0.60	9.60
		400	5.35	0.00	23.61	1.61	0.45	18.44
		600	5.81	0.10	35.99	1.06	0.38	10.74
		800	4.26	0.13	35.67	1.07	0.36	11.95
13/01/2011	#21 (E151)	20	44.75	1.54	114.13	0.72	1.38	2.58
		35	39.99	1.82	73.37	0.77	0.94	2.29
	53.75°S, 38.98°W	50	48.57	2.03	94.66	1.24	1.36	1.91
		75	25.63	0.91	68.56	0.98	1.17	-
		100	64.06	1.91	114.03	2.33	1.32	1.51
		150	73.04	1.59	62.83	7.70	1.28	12.20

Table 2: SAPS samples: The particulate Fe (PFe), Mn (PMn), and Al (PAl) concentrations in the top 150 m of the water column at the 14 sites visited during JR247. The particulate fraction, P, is the sum of leachable ~~particulate~~ (L~~P~~) and refractory ~~particulate~~ (R~~P~~). Because of low concentrations, the leachable ~~particulate~~ fraction is indicated in percent of the P fraction. Additional information covers sampling date, site (station) ID, event number, latitude and longitude, and water column depth. (Depths marked by * indicate that the polycarbonate filter was corrupted after retrieving the SAPS)

Date	Site ID	Depth		Particulate (nmol L^{-1})			Leach. Part. (% of P)	
	Lat. & Lon.	(m)	PFe	PMn	PAl	L~~P~~Fe	L~~P~~Mn	L~~P~~Al
25/12/2010	#1/2 (E22)	20	5.17	0.08	4.82	0.37	2.39	1.65
	53.70°S, 38.21°W	50*	9.12	0.14	7.91	0.27	2.61	1.47
	(322 m)	150*	76.61	1.09	66.91	6.26	2.74	4.65
26/12/2010	#3 (E31)	20	6.62	0.09	6.64	0.02	3.30	0.79
	53.85°S, 39.14°W	50	267.48	3.85	162.59	1.48	0.79	0.65
	(287 m)	150	4.36	0.06	4.26	0.07	1.55	1.93
31/12/2010	#4/5 (E72)	20	8.52	0.12	7.99	0.51	1.68	2.62
	53.49°S, 37.71°W	50	15.15	0.23	12.96	0.56	2.44	2.74
	(1917 m)	150	2.33	0.03	2.15	0.65	1.78	2.42
02/01/2011	#6 (E80)	20	85.74	1.11	59.05	1.60	2.28	4.50
	53.99°S, 36.37°W	50	17.76	0.24	8.87	-	-	-
	(208 m)	150	137.39	2.02	98.54	3.46	0.91	2.81
03/01/2011	#7/8 (E88)	20	1.95	0.02	0.87	0.13	2.97	4.99
	54.10°S, 35.46°W	50	1.67	0.02	0.92	0.08	4.35	4.24
	(330 m)	150	1.23	0.02	0.71	0.19	2.11	5.13
04/01/2011	#9/10 (E96)	20	20.91	0.08	15.74	0.56	5.01	3.24
	54.26°S, 35.35°W	50	19.16	0.27	15.58	0.45	1.22	2.51
	(263 m)	150	54.06	0.77	48.10	1.08	1.65	2.08
05/01/2011	#11/12 (E100)	20*	1.49	0.01	0.86	0.18	4.42	2.92
	54.62°S, 34.81°W	50	0.87	0.01	0.60	0.27	6.63	4.20
	(747 m)	150	1.76	0.03	1.08	0.37	4.38	3.33
06/01/2011	#13 (E106)	20	2.75	0.03	1.78	0.63	3.13	4.29
	54.53°S, 35.27°W	50	4.11	0.05	3.07	0.44	2.04	2.76
	(133 m)	100	10.28	0.15	7.62	0.46	1.70	2.54
07/01/2011	#14 (E114)	20	2.80	0.04	1.84	0.07	1.58	3.29
	54.56°S, 35.59°W	50	1.41	0.02	0.97	0.10	2.57	3.92
	(263 m)	150	31.34	0.46	26.92	0.72	1.57	2.28
08/01/2011	#15/16 (E120)	20	24.54	0.37	22.91	0.85	3.95	1.88
	53.62°S, 36.34°W	50	27.72	0.40	23.23	0.43	3.65	1.36
	(852 m)	150	4.74	0.07	3.94	0.90	4.31	1.06

10/01/2011	#17 (E134)	20	10.43	0.14	8.09	0.34	1.66	2.41
	53.90°S, 36.57°W	50	43.04	0.60	38.79	1.34	1.07	1.67
	(209 m)	150	207.48	3.10	194.88	1.72	0.82	1.50
11/01/2011	#18 (E139)	20	95.52	1.32	88.39	1.39	1.82	1.93
	54.10°S, 36.25°W	50	37.43	0.52	35.33	1.16	1.29	1.85
	(276 m)	150	28.00	0.41	23.60	1.26	2.35	2.27
12/01/2011	#19/20 (E142)	20	97.60	1.52	97.10	0.16	1.66	0.33
	53.54°S, 38.11°W	50	90.96	1.42	92.89	0.39	1.98	0.80
	(1741 m)	150	7.41	0.12	6.37	0.74	8.25	2.75
13/01/2011	#21 (E152)	20	50.75	0.85	52.78	0.06	2.99	0.12
	53.75°S, 38.98°W	50	59.59	0.93	59.98	0.05	2.15	0.09
	(269 m)	150	153.48	2.34	89.63	3.14	1.10	2.94

Table 3: Illustrates the different elemental ratios of earth crust, sediment, suspended (SAPS), faecal pellet, and biogenic particles (average phytoplankton species).

particle	Fe/Mn (mol mol^{-1})	Fe/Al (mol mol^{-1})	Mn/Al (mol mol^{-1})	source
crustal	58.00	0.20	0.0035	a
sediment	51.50	0.34	0.0066	This study
suspended (SAPS)	68.00	1.25	0.0171	This study
faecal pellets	70.65	0.48	0.0069	This study
phytoplankton	1.70	-	-	b

a) Wedepohl, 1995; b) Ho et al., 2003

Table ~~3~~4: Sediment core samples: Particulate iron (SFe), aluminum (SAl), and manganese (SMn) concentrations in shelf sediments collected during JC055 in January and February 2011. Pore water data retrieved additionally from these three cores are listed for Fe (Fe_{PW}) and Mn (Mn_{PW}). Additional information are event number (MC…), latitude + longitude, and water column depth.

Station ID Lat. & Lon.	Depth (cm)	SFe (mol kg-1)	SAl (mol kg-1)	SMn (mmol kg-1)	Fe_{PW} (µmol kg-1)	Mn_{PW} (µmol kg-1)
#S1 (MC33)	0.5	0.58	1.77	11.56	3.01	2.29
54.16°S, 37.98°W	1.5	0.61	1.74	11.52	17.47	0.84
(257 m)	2.5	0.59	1.77	11.78	110.90	0.28
	3.5	0.6	1.86	12.05	106.24	0.53
	4.5	0.58	1.72	11.82	94.09	0.34
	5.5	0.59	1.86	12.04	82.79	0.27
	9	0.56	1.72	11.19	32.98	0.00
	15	0.55	1.74	11.15	2.44	0.06
	25	0.53	1.6	10.81	0.80	0.16
#S2 (MC34)	0.5	0.64	1.77	11.42	1.53	0.87
54.16°S, 37.94°W	1.5	0.6	1.79	11.73	/	/
(247 m)	2.5	0.58	1.76	11.81	0.97	0.24
	6.5	0.59	1.83	12.23	11.19	0.26
	10.5	0.58	1.8	11.78	14.28	0.25
	14.5	0.54	1.6	10.83	3.59	0.33
	16.5	0.56	1.72	11.22	2.27	0.31
#S3 (MC35)	0.5	0.61	1.67	11.42	1.46	0.43
54.15°S, 37.97°W	1.5	0.59	1.76	11.7	28.94	0.35
(254 m)	2.5	0.58	1.76	11.7	91.52	0.37
	3.5	0.59	1.81	12.03	40.16	0.44

5.5	0.57	1.78	11.58	49.37	0.56
8.5	0.59	1.82	11.65	67.92	0.52
17	0.54	1.69	10.8	3.87	0.34
19	0.55	1.67	10.86	1.82	0.12
25	0.55	1.77	11.19	2.73	0.36
29	0.56	1.79	11.19	5.64	0.16

Table ~~4~~5: Krill faecal pellets: Particulate (P) and leachable ~~particulate~~ (L~~P~~) concentrations for Fe, Mn, and Al determined for the 27 individual krill faecal pellet samples collected during 9 krill incubation experiments on-board RRS *James Clark Ross* (JR247). The particulate fraction, P, is the sum of leachable ~~particulate~~ (L~~P~~) and refractory ~~particulate~~ (R~~P~~). Because of low concentrations, the leachable ~~particulate~~ fraction is indicated in percent of the P fraction.

# Sample	pellet weight (mg)	PFe ($\mu g\ mg^{-1}$)	PAl ($\mu g\ mg^{-1}$)	PMn ($ng\ mg^{-1}$)	L~~P~~Fe (%)	L~~P~~Al (%)	L~~P~~Mn (%)
1	4.87	0.88	1.06	12.5	6.33	8.83	13.24
2	2.18	1.33	1.68	16.7	3.02	8.81	8.22
3	4.26	1.07	1.90	17.8	5.37	3.27	11.81
4	1.91	5.19	5.53	76.1	2.15	1.95	5.68
5	1.41	2.70	2.84	39.1	2.46	1.59	3.54
7	7.80	67.1	64.2	998.3	2.93	2.21	3.25
8	0.99	2.71	2.42	35.0	3.76	4.59	5.99
10	1.48	6.42	4.89	71.6	0.29	4.83	0.91
13	2.79	4.13	3.11	50.3	0.36	5.07	1.53
15	0.77	37.3	38.1	531.1	2.03	2.80	6.21
16	1.21	6.35	6.22	81.2	1.24	7.47	3.13
18	12.27	40.0	36.6	582.5	3.95	2.07	4.29
19	2.19	11.2	9.49	146.9	0.15	2.03	1.07
22	2.43	48.1	49.7	721.5	0.81	2.32	0.98
40	3.35	22.8	22.0	337.4	5.51	3.21	5.50
41	8.55	6.91	7.14	103.1	1.11	1.88	4.31
42	3.5	25.7	24.8	376.2	5.09	2.98	5.29
45	0.40	3.96	4.43	43.3	1.27	13.90	1.46
47	7.65	3.63	3.92	52.7	0.34	0.68	3.65
48	0.63	3.06	3.21	34.1	0.05	4.22	0.76
49	4.42	29.6	28.5	438.4	1.65	2.93	1.95
50	7.46	2.31	2.37	34.6	0.36	0.51	2.78
51	5.18	28.0	27.1	431.3	1.85	2.60	2.01
62	1.20	4.63	4.68	68.0	0.31	1.78	0.47
68	2.25	44.0	40.2	667.4	4.84	1.95	4.77
69	1.66	43.6	44.8	663.7	5.66	2.13	5.46
71	3.47	35.3	36.4	557.7	1.50	1.99	1.76

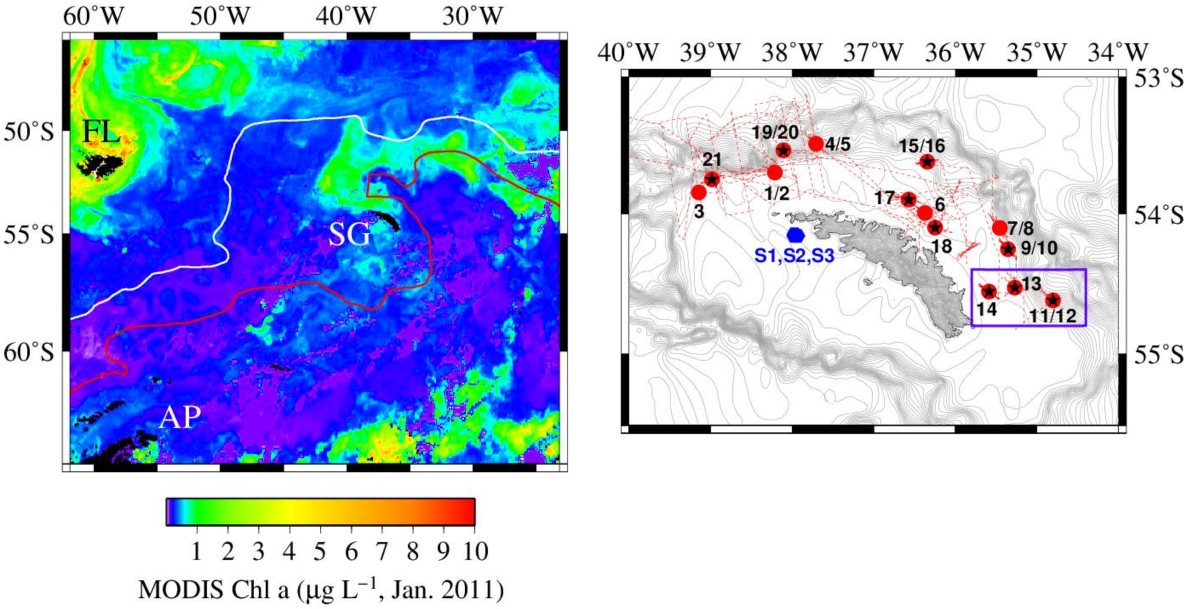

Figure 1: (Left figure) Locations of Falkland Islands (FL), South Georgia (SG), and Antarctic Peninsula (AP) in the Atlantic sector of the Southern Ocean. South Georgia is located between the Antarctic Polar Front (PF, white line) and the Subantarctic Circumpolar Current Front (SACCF, red line). The colour bar represents the Chlorophyll a (Chl a) content recorded by the MODIS satellite in January 2011. (Right figure) The region around SG and the **OTE** (black stars) and **SAPS** sampling sites (red points) visited during JR247. The red dashed line illustrates the cruise track of JR247. The three sediment sampling sites S1, S2, and S3 visited during JC055 are shown by blue hexagons. The purple box indicates the W-E transect from shelf site #14 via site #13 to the shelf edge site #11/12. The ocean bathymetry of the region was plotted using the GEBCO bathymetric data set. The shelf of South Georgia is between 100 and 250 m deep and extends about 30 to 100 km (shelf edge indicated by high density of isobaths).

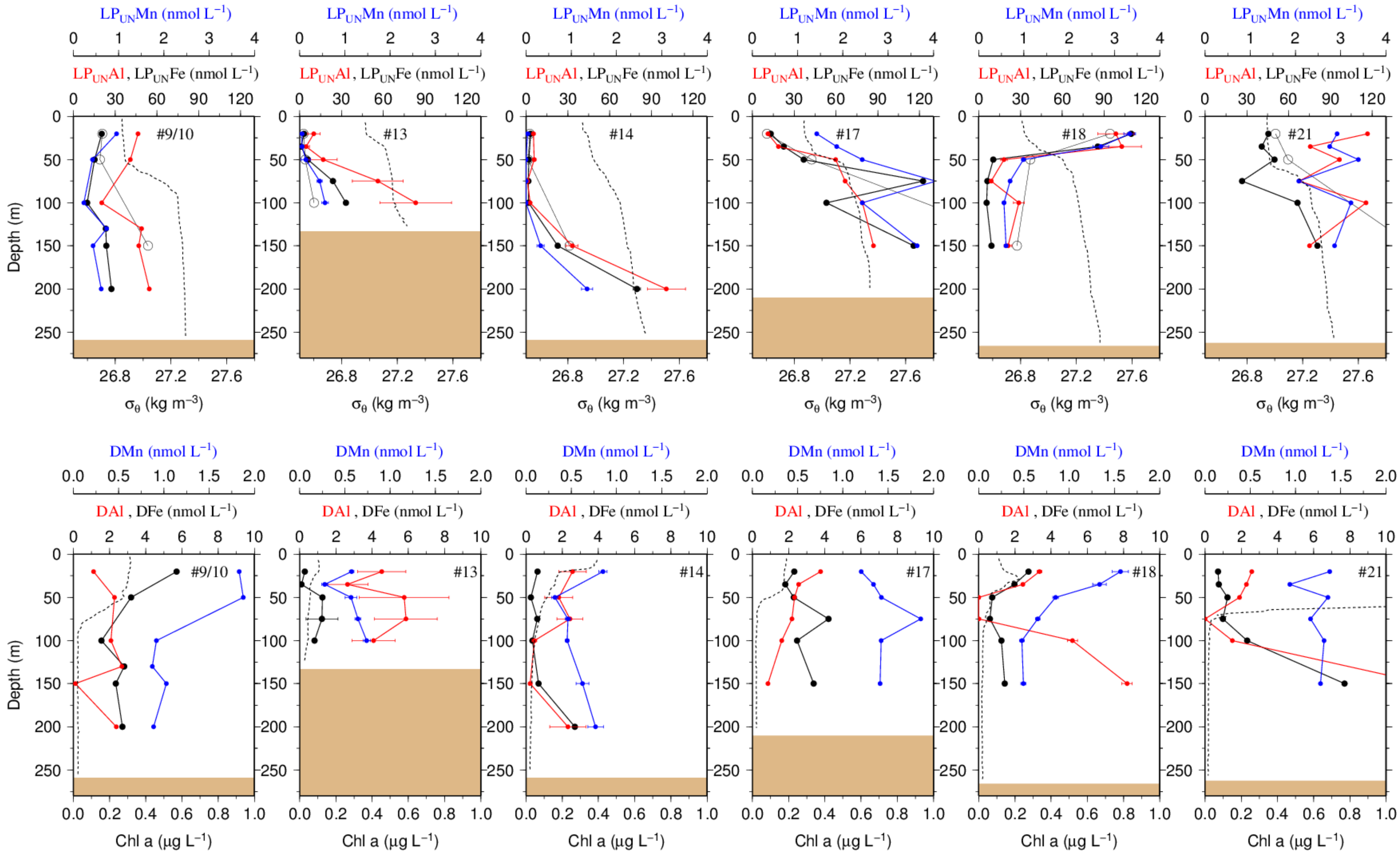
$LP_{UN}Mn$ (nmol L^{-1})
$LP_{UN}Al$, $LP_{UN}Fe$ (nmol L^{-1})
#9/10
#13
#14
#17
#18
#21
Depth (m)
σ_θ (kg m^{-3})
26.8
27.2
27.6
DMn (nmol L^{-1})
DAl , DFe (nmol L^{-1})
Chl a (µg L^{-1})
0 1 2 3 4
0 30 60 90 120
0 50 100 150 200 250
0.0 0.5 1.0 1.5 2.0
0 2 4 6 8 10
0.0 0.2 0.4 0.6 0.8 1.0

Figure 2: (Upper row) **OTE-seawater samples:** Distribution of leachable particulate iron (LP$_{\mathrm{Un}}$Fe in black), manganese (LP$_{\mathrm{Un}}$Mn in blue), and aluminium (LP$_{\mathrm{Un}}$Al in red) concentrations in the water column of stations located on the island shelf (125 m – 270 m water depth). **SAPS samples:** The particulate Fe (PFe) fraction retrieved by SAPS is illustrated with open black circles and corresponds to the ~~concentration labels~~same axis as ~~of~~ LP$_{\mathrm{Un}}$Fe. Concentrations above 120 nmol L^{-1} are listed in Table 1 and 2. Error bars represent the standard deviation of the analysis. Density sigma-theta (σ_θ) in kg m^{-3} is illustrated by the black dashed line. (Lower row) **OTE-seawater samples:** Dissolved iron (DFe), manganese (DMn), and aluminium (DAl) are represented by the same colour code as above. Dashed lines illustrate Chlorophyll a (Chl a) content of the water column recorded by the CTD fluorometer.

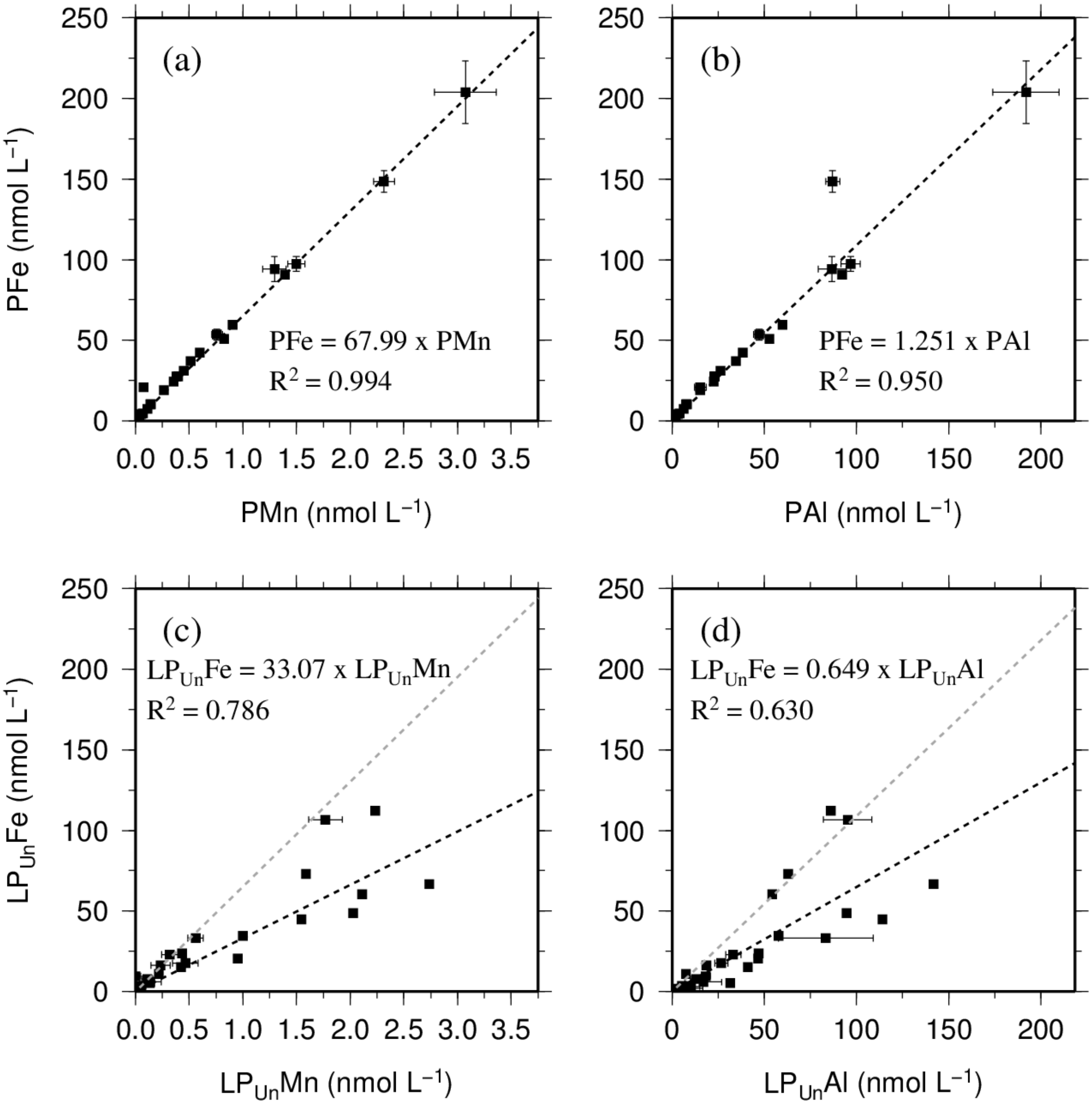

Figure 3: Relationship of the entire data set for the particulate fraction of Fe, Mn, and Al in particulates (P) retrieved using SAPS ((a) and (b)) and the leachable particulate fraction (LP_{UN}) estimated from unfiltered and dissolved seawater samples collected using OTE bottles ((c) and (d)). Error bars represent the standard deviation of the analysis. The linear regression of each relationship is illustrated by a dashed black line, the formula, and the R^2. The grey dashed line in c. and d. represents the linear relationship of particulate trace meals (P) shown in (a) and (b).

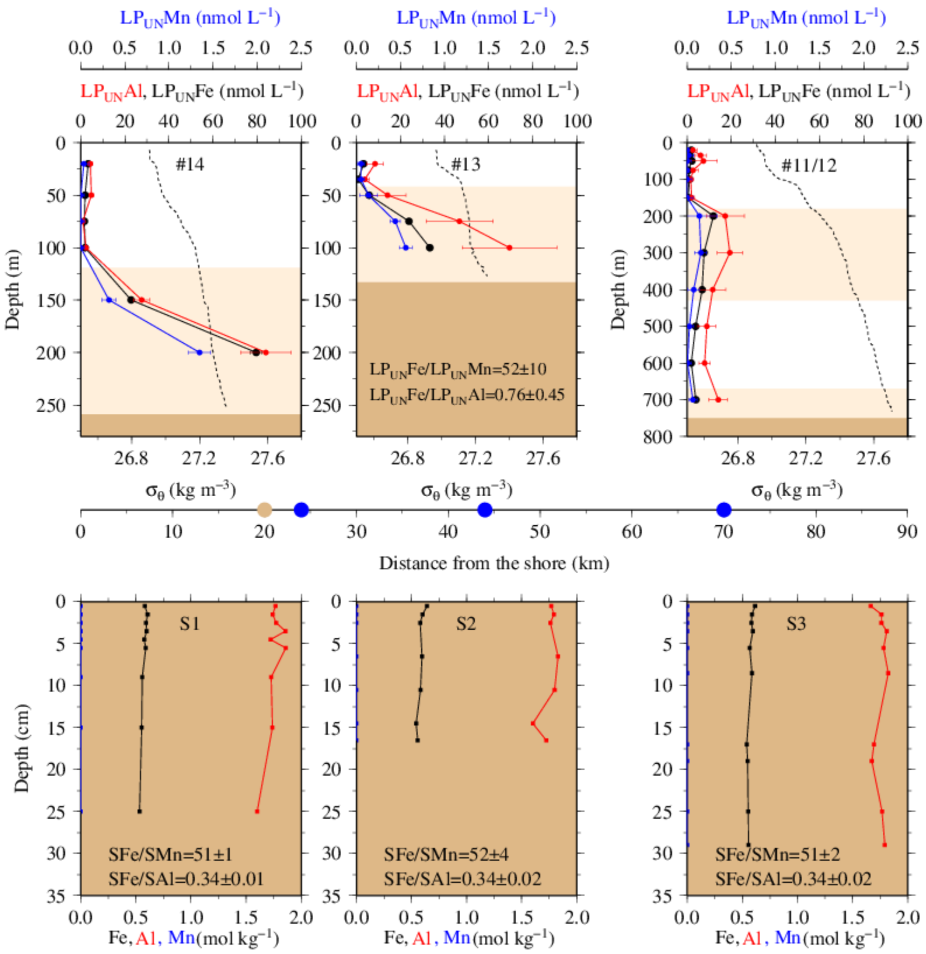

Figure 4: (Upper row) **OTE-seawater samples:** From left to right, concentrations of leachable particulate iron (LP$_{\mathrm{Un}}$Fe), aluminium (LP$_{\mathrm{Un}}$Al), and manganese (LP$_{\mathrm{Un}}$Mn) of unfiltered seawater samples for the two shelf sites #14, #13 and the shelf edge site #11/12 (Note different depth scaling). Error bars represent the standard deviation of the analysis. Water density (sigma-theta (σ_θ)) is shown by the dashed black line. Brown areas represent sediments and pink areas the zone of resuspended sediment particles in the water column. Diagram 14 (left) contains the average LP$_{\mathrm{Un}}$Fe/LP$_{\mathrm{Un}}$Al and LP$_{\mathrm{Un}}$Fe/LP$_{\mathrm{Un}}$Mn ratio of particles in seawater samples collected within the pink layers. (Lower row) **Sediment core samples:** Diagram S1, S2 and, S3 displays the Fe, Mn, and Al content in the three sediment cores. Shown are average SFe/SAl and SFe/SMn ratios (mol/mol) of particles from the surface layer for site S1, S2, and S3. Dots on the distance scaling in the middle represent the distance of each water column station (blue) and sediment core (brown) station to the nearest shore.

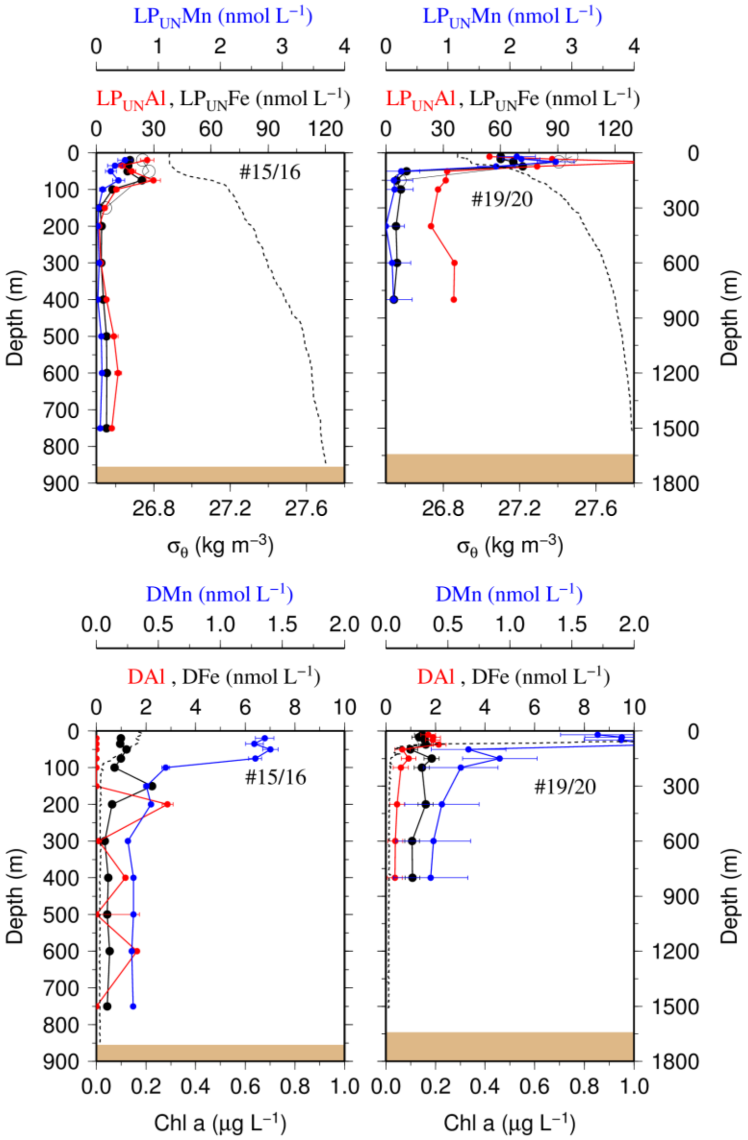

Figure 5: (Upper row) **OTE-seawater samples:** Distribution of leachable particulate manganese (LP$_{\text{Un}}$Mn in blue), iron (LP$_{\text{Un}}$Fe in black), and aluminium (LP$_{\text{Un}}$Al in red) concentrations in the water column of the two other stations located on the island shelf edge (> 700 m water depth). **SAPS samples:** The particulate Fe (PFe) is illustrated by black circles and corresponds to the concentration labels of LP$_{\text{Un}}$Fe. Error bars represent the standard deviation of the analysis. Sigma-theta (σ_θ) is illustrated by the black dashed line. (Lower row) **OTE-seawater samples:** Dissolved manganese (DMn), iron (DFe), and aluminium (DAl) are represented by the same colour code as for the upper row. Dashed line illustrates the Chl a content of the water column recorded by the CTD mounted fluorometer.

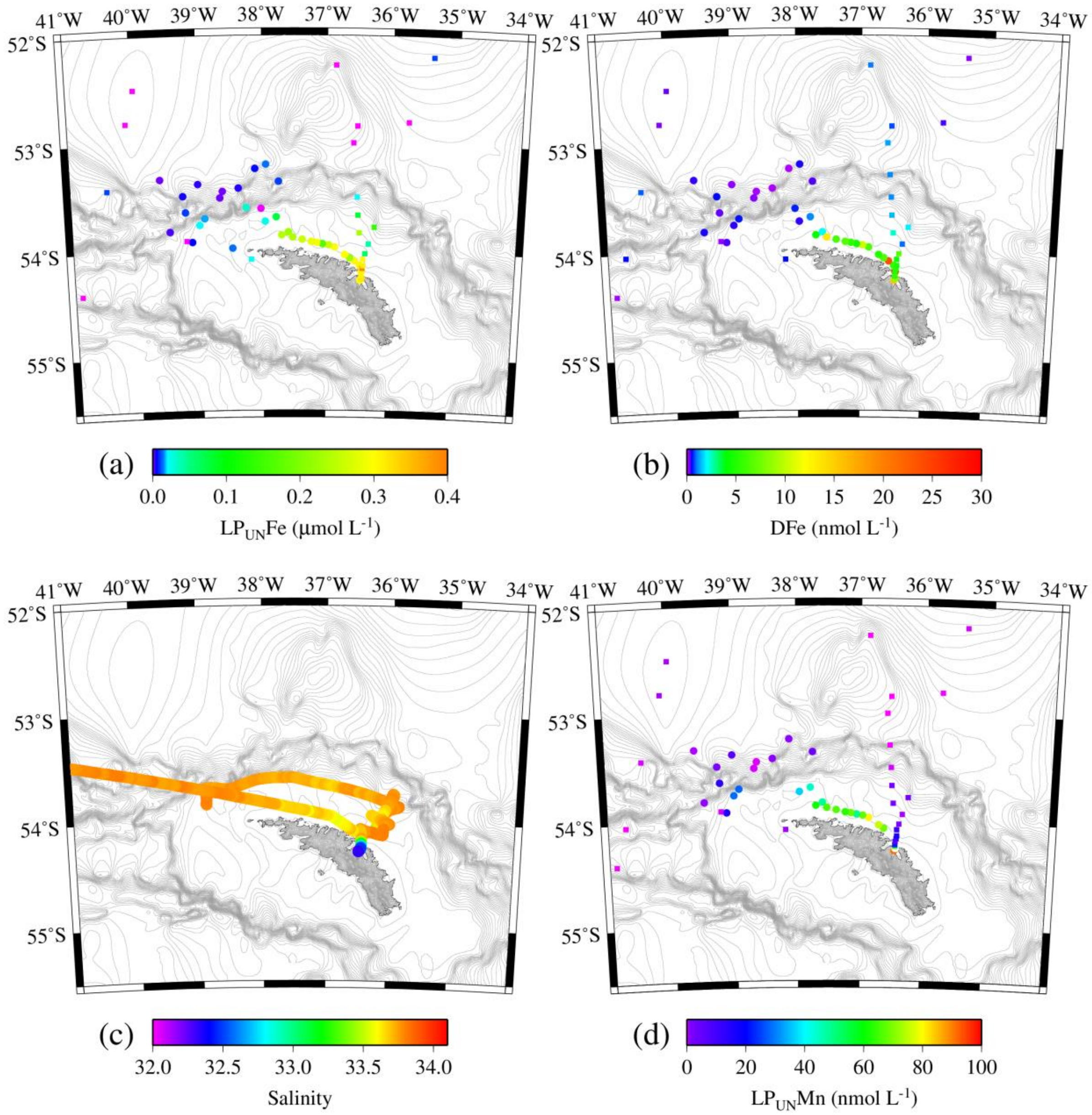

Figure 6: Tow fish-seawater samples: Concentrations of leachable particulate Fe (LP$_{UN}$Fe) of unfiltered seawater samples (a), dissolved Fe (DFe) (b), Salinity (c) and leachable particulate Mn (LP$_{UN}$Mn) in unfiltered seawater samples (d) in surface waters collected during JR247 (circles) and JR274 (squares) around South Georgia. The highest LP$_{UN}$Fe concentration was recorded in a single sample in Cumberland Bay reaching 2.2 µmol L^{-1}. Because of generally lower concentrations we excluded this data point in panel (a). Isobath are represented by grey lines (GEBCO – Gridded Bathymetry Data).

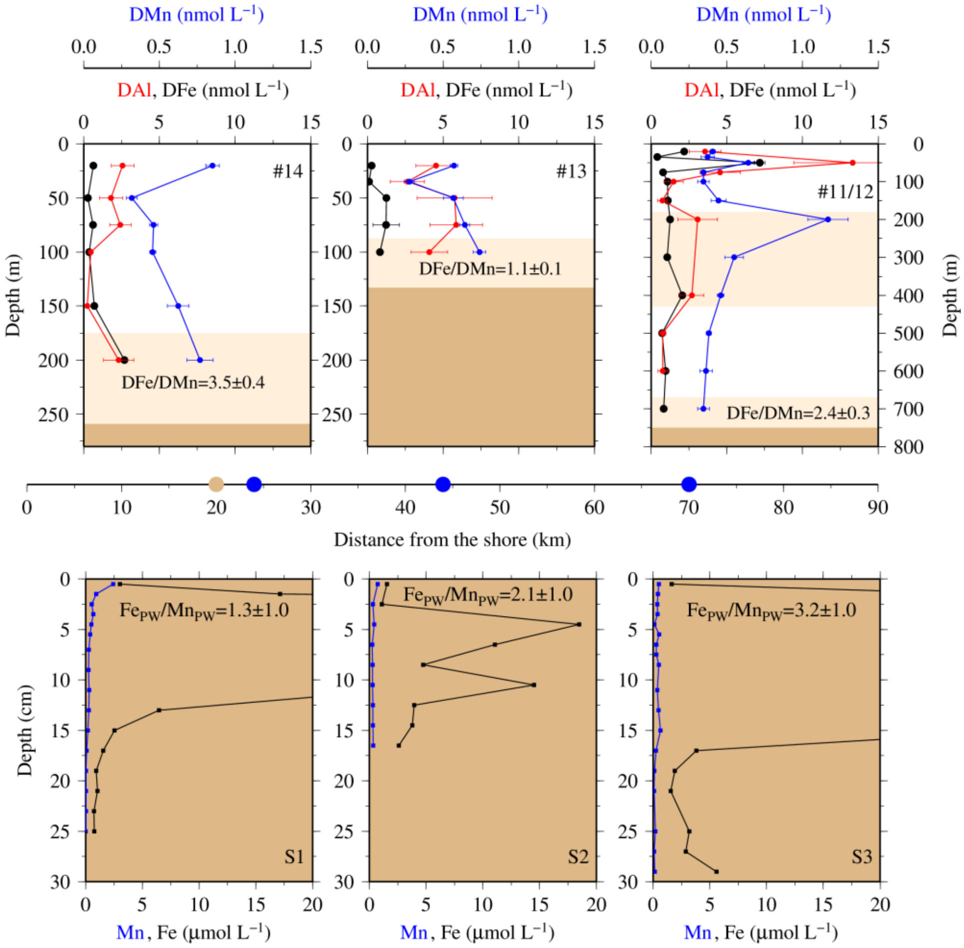

Figure 7: (Upper row) **OTE-seawater samples:** From left to right, concentrations of dissolved iron (DFe), aluminium (DAl), and manganese (DMn) for the two shelf sites (#14, #13) and the shelf edge site (#11/12). Note different depth scaling. Error bars represent the standard deviation of the analysis. Pink areas represent the zone of resuspended sediments in the water column. The DFe/DMn ratios of the seawaters collected within the pink zone is indicated. (Lower row) **Sediment core samples:** Diagram S1, S2 and, S3 displays the Fe (black), and Mn (blue) content in pore waters of the three sediment cores. Values off-axis can be found in Table ~~3~~4. Shown are average Fe_{PW}/Mn_{PW} ratios (mol/mol) of top surface layer (1 cm) for site S1, S2, and S3. Dots on the distance scaling in the middle represent the distance of each water column station (blue) and sediment core (brown) station to the nearest shore.

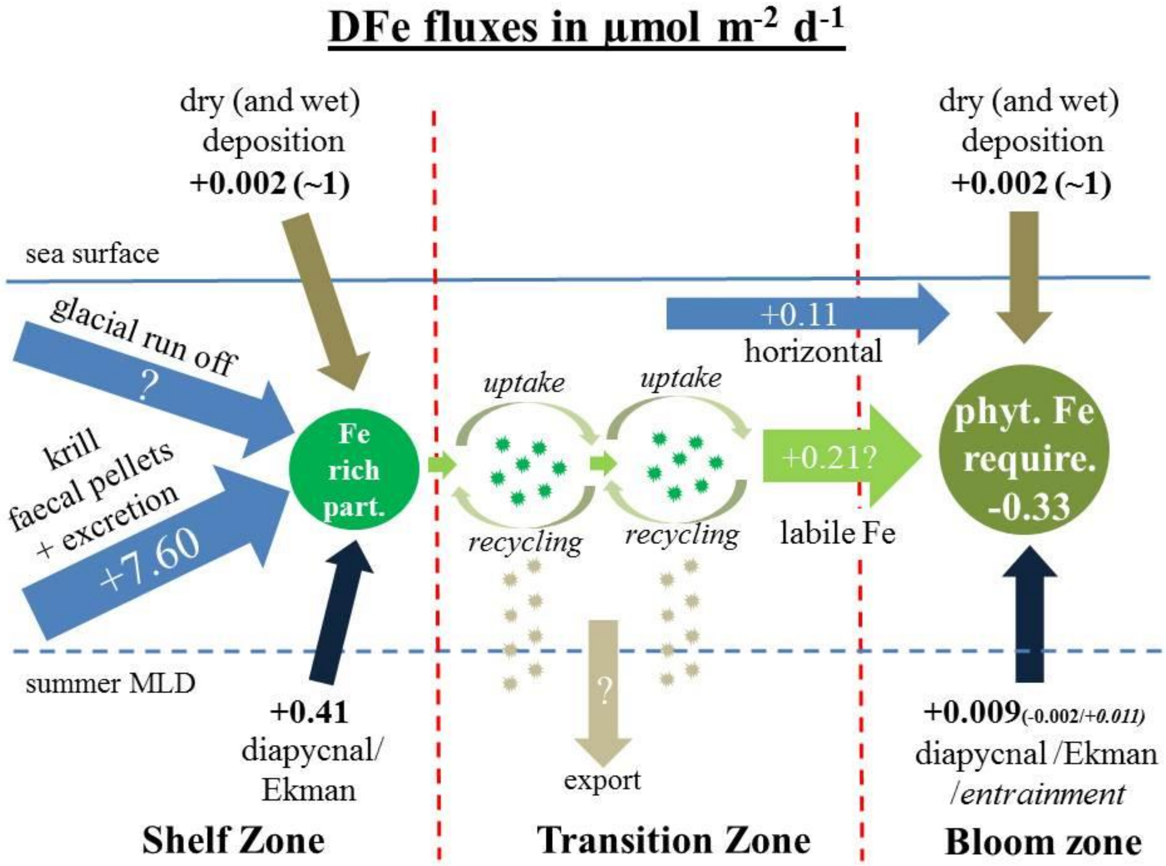

Figure 8: Sketch of DFe fluxes on the shelf, in the transition zone and in the downstream blooming region, separated by the red dashed lines. (left sketch) Describes the dissolved Fe fluxes on the shelf that together generate Fe rich biogenic and lithogenic particles (dark green). These are transferred offshore (light green arrows) following the ACC to open ocean sites (sketch in the middle). Iron enriched particles (dark green) in the transition zone are recycled and supplement DFe requirements of the phytoplankton community in the transition zone. During each cycle of recycling and uptake an unknown Fe fraction is lost by vertical export. (right sketch) Describes the dissolved Fe fluxes in the blooming zone.

Supplementary Material of

Mechanisms of dissolved and labile particulate iron supply to shelf waters and phytoplankton blooms off South Georgia, Southern Ocean

Christian Schlosser, Katrin Schmidt, Alfred Aquilina, William B. Homoky, Maxi Castrillejo, Rachel A. Mills, Matthew D. Patey, Sophie Fielding, Angus Atkinson, and Eric P. Achterberg

Supplementary Text

Text S1: Seawater sampling and analysis

Water column samples were collected using trace metal clean OTE bottles deployed on a Kevlar line. The OTE bottles were transferred into the clean container where all sample handling was performed. Dissolved and total dissolvable seawater samples were acidified immediately with concentrated trace metal grade nitric acid (HNO_3, UpA, Romil) to pH 1.66 (22 mmol H^+ L^{-1}). Acidified seawater samples were shipped to the National Oceanography Centre Southampton and analyzed by isotope dilution (ID) and standard addition inductively coupled plasma - mass spectrometry (ICP-MS).

The preconcentration and ICP-MS analysis was adapted from the method outlined by Rapp et al. (2017). Approximately one year after collection, 12 mL of acidified seawater was transferred into 30 mL fluorinated ethylene propylene (FEP) bottles and spiked with a spike solution containing mainly the artificially enriched isotope of iron (^{57}Fe). For the analysis of Al, and Mn a series of four standard additions were performed on every tenth sample. To obtain equimolar conditions between the spike and the natural seawater concentration, larger amounts of spike was added to the total dissolvable seawater samples. All samples were irradiated with strong ultraviolet light for 3.5 hours. Subsequently, the sample solution was buffered to pH 6.4 using a 2 M ammonium acetate solution (pH9.2, Fisher Optima grade ammonia and acetic acid, glacial). Immediately after buffer addition the solution was preconcentrated using an automated system (Preplab, PS Analytical) that was equipped with a metal chelating resin (WACO) resin (Kagaya et al., 2009). Any remaining seawater salts were rinsed off using deionized water (> 18 MΩ cm, MilliQ, Millipore). The metals retained on the resin were eluted using 1 mL of a 1 M sub-boiled HNO_3 solution, which was collected in acid cleaned 4 mL polypropylene vials. The collected vials were placed into the auto-sampler of the ICP-MS (Element XR, Thermo).

The difference between the total dissolvable (TDM) and dissolved metal (DM) concentrations was used to determine the particulate concentration ($LP_{UN}M$ = TDM – DM). It should be noted that this particulate fraction represents the amount of Fe ($LP_{UN}Fe$), Al ($LP_{UN}Al$), and Mn ($LP_{UN}Mn$) re-dissolved from particles within 1 year after the addition of 22 mmol H^+ L^{-1}. This means acid-inert minerals (e.g. zircon) and their associated trace metals likely did not contribute to the particulate metal concentration.

Certified seawater standards (SAFe D2 and GEOTRACES D) were preconcentrated and analyzed with each batch of samples, in order to validate our sample concentration. Values obtained by us for the certified seawater standards agreed with reported values for the GEOTRACES and the SAFe standard seawater (SAFe D2: 0.92 ± 0.02 nmol Fe L^{-1} (certified 0.90 ± 0.02 nmol Fe L^{-1}), GEOTRACES D: 1.00 ± 0.04 nmol Fe L^{-1} (certified 0.95 ± 0.05 nmol Fe L^{-1}). The precision for replicate analyses was between 1-3%. The buffer blank was 0.056 ± 0.016(σ_{bl}) nmol Fe L^{-1}, and the limit of detection (3 x standard deviation of the blank) was determined as 0.061 ± 0.020(σ_{bl}) nmol Fe L^{-1}.

Certified reference materials (crm), NIST 1573a and Tort 2, were digested and analysed with each batch of suspended particle and faecal pellet samples, in order to validate our sample concentration. Values obtained agreed with reported values of the crm (NIST

1573a: 423 ± 5 mg Fe kg^{-1} (certified 368 ± 7 mg Fe kg^{-1}), 244 ± 2 mg Mn kg^{-1} (certified 246 ± 8 mg Mn kg^{-1}), 550 ± 1 mg Al kg^{-1} (certified 598 ± 12 mg Al kg^{-1}); Tort-2: 117 ± 2 mg Fe kg^{-1} (certified 105 ± 13 mg Fe kg^{-1}), 13 ± 1 mg Mn kg^{-1} (certified 14 ± 1 mg Mn kg^{-1})).

Text S2: Sediment and porewater sampling and analysis

Sediment cores with an undisturbed sediment-seawater interface were immediately transferred to a N_2-filled glove bag in a temperature-controlled laboratory to simulate ambient bottom water temperatures (approximately 4°C). Sediments were manually extruded at depth intervals of 1 or 2 cm into a polycarbonate ring, and sectioned using a polytetrafluoroethylene (PTFE) sheet that was cleaned with deionised water between each application. Porewater was separated from each sediment section by centrifugation at 9,000 g at 4°C under N_2 for 10 minutes; the supernatant porewaters were filtered under N_2 through 0.2 µm cellulose nitrate syringe filters (Whatman, UK). Aliquots of each porewater sample were collected in acid-cleaned LDPE bottles (Nalgene) and acidified to pH <2 by adding 2 µL of concentrated hydrochloric acid (HCl, UpA, Romil) per 1 mL of sample; acidified samples were stored refrigerated prior to analysis at NOCS. Conjugate sediments were freeze dried on board and stored at room temperature, pending analysis at the NOCS.

Sub-samples (~100 mg) of the bulk, homogenized sediments were completely dissolved using hot aqua regia (HNO_3+HCl) followed by hot hydrofluoric-perchloric acid ($HF-HClO_4$) mixtures and finally diluted in 0.6M HCl as described elsewhere (Homoky et al., 2011) . The acid digests were analysed by ICP-OES (Perkin Elmer Optima 4300DV). Calibration standards were matrix-matched and blank and instrument drift were monitored and corrected for by including calibration blanks and multi-element standards with each batch of 10 analyses. To ascertain the accuracy of the method certified reference material MAG-1 (United Sates Geological Survey) was analysed with each batch of samples. The values measured in our laboratory are in close agreement with the certified values: 42.978 ± 3.155 g

Fe kg^{-1} (certified 47.600 ± 4.200 g Fe kg^{-1}); 715 ± 9 ng Mn g^{-1} (certified 760 ± 69 µg Mn kg^{-1}); and 76.605 ± 2.740 g Al kg^{-1} (certified 86.800 ± 1.600 g Al kg^{-1}).

Acidified porewater samples were analysed for a suite of major and trace elements, by ICP-OES (Perkin Elmer Optima 4300 DV). Elements including Fe and Mn were measured at 50-fold dilutions of the porewater sample in 0.6M HCl. Calibration standards were matrix matched and blank and instrument drift were monitored and corrected for by including calibration blanks and multi-element standards for each batch of ten analyses. The instrument limits of detection (LD, 3 x standard deviation of acid blanks) were 1.25 µg Fe kg^{-1} and 0.08 µg Mn kg^{-1}.

Text S3: Calculation of dissolved Fe and Mn fluxes from shelf sediment porewaters

The calculation of pore water Fe and Mn fluxes follows the approach of Boudreux and Scott (1978), who described the flux of pore water Mn(II) by diffusion and reaction through an oxygenated surface layer in marine sediments.

$$\boldsymbol{J = \frac{\varphi(D_s k_1)^{0.5} C_p}{sinh((k_1/D_s)^{0.5} L)}}$$

Where *J* is the flux (g cm^{-2} s^{-1}) of Mn(II) from sediment pore water to bottom water, *L* is the thickness (cm) of the oxygenated surface layer where Mn(II) is removed from the pore water by oxidative precipitation in the sediment, and C_p is the concentration (g cm^{-3}) of Mn(II) in the pore water beneath *L* relative to the overlying bottom water. The diffusive rate constant, D_s (cm^2 s^{-1}), is derived from sediment porosity (φ), and the Mn(II) oxidation rate constant, k_1 (s^{-1}), is estimated from field studies (Boudreux and Scott, 1978). This method has more recently been adopted for the determination of pore water Fe(II) fluxes (Homoky et al., 2013; Raiswell and Anderson, 2005) using the Fe(II) oxidation kinetics of (Millero et al., 1987) to derive k_1, and has been favourably compared with incubated flux determinations from shelf sediments (Homoky et al., 2012).

We use measured and estimated values for scalar terms for the flux calculations that are summarised in Supplementary Table S1 to investigate the potential for pore water fluxes of Fe and Mn from sites S1, S2 and S3. Sediment porosity (φ) was measured by the change in wet sediment mass after drying sliced core samples. Oxygen penetration depth (L) was measured from a single sediment core from site S3 with a Unisense microsensor apparatus following Homoky et al. (2013), and in the absence of multiple determinations is extrapolated to each core site. Diffusion coefficients (D_S) are a derived from measurements of φ after Boudreau and Scoot (1978). The oxidation rate constant (k_1) for Mn(II) is also derived from Boudreau and Scoot (1978). For Fe(II), k_1 is calculated from values of bottom water $O_{2,}$ temperature (0 °C), salinity (34) and an estimated pore water pH of 7.5 (Homoky et al., 2012), following Millero et al. (1987) (Homoky et al., 2013; Homoky et al., 2012; Raiswell and Anderson, 2005). Values of C_P are for measured data (at 0.5 and 1.5 cm depth) closest to the depth of L from each core site. Corresponding fluxes of pore water Fe (<0.1 to 44.4 µmol m^2 d^{-1}) and Mn (0.6 to 4.1 µmol m^2 d^{-1}) fall within the range of fluxes measured from continental margin sediments of the northeast Pacific (John et al., 2012; McManus et al., 2012) and demonstrate South Georgia shelf sediments are also likely to be an important source of Fe and Mn to the water column.

Text S4: Estimation of phytoplankton Fe requirements and Fe fluxes

The Fe requirements of the phytoplankton community within the bloom were estimated by combining satellite derived marine net primary productivity data (NPP = 62 ± 21 mmol C m^{-2} d^{-1} (Ma et al., 2014)) with an average intracellular Fe:C ratio (5.2 ± 2.8 µmol Fe mol^{-1} C^{-1} (Strzepek et al., 2011)). NPP was estimated from satellite-derived information using a phytoplankton pigment absorption based model (Ma et al., 2014). The applied NPP rate corresponded to an average chlorophyll a content in the euphotic zone of ~ 4 ug L^{-1}. There are several literature values for Fe:C ratio estimates ranging from 6 – 14 µmol Fe mol^{-1} C^{-1} under natural non Fe-fertilized and 10 – 40 µmol Fe mol^{-1} C^{-1} under Fe-fertilized conditions for Southern Ocean diatoms, autotrophic flagellates, and heterotrophic flagellates (Twining et al., 2004). Lab based incubation experiments using coastal phytoplankton species, such as *Dunaliella tertiolecta, Pyramimonas parkeae, Nannochloris atomus, Pycnococcus provasoli, Tetraselmis* sp., *Gymnodinium chlorophorum, Prorocentrum mimimum, Amphidinium carterae, Thoracosphaera heimii, Emiliania huxleyia, Gephyrocapsa oceanica, Ditylum brightwellii, Thalassiosira weissflogii, Nitzschia brevirostris,*and *Thalassiosira eccentric,* reviled an average value of ~ 51 µmol Fe mol^{-1} C^{-1} (Ho et al., 2003), while Southern Ocean phytoplankton species including *Phaeocystis antarctica* (clone AA1), *Fragilariopsis kerguelensis, Thalassiosira Antarctica, Eucampia Antarctica,* and *Proboscia inermis* were an order of magnitude lower between 1.8 – 8.6 (Strzepek et al., 2011). Because most phytoplankton species from the Southern Ocean are very well adapted to the very low Fe water content, we decided to apply the low Fe:C ratios provided by Strzepek et al. (Strzepek et al., 2011). The Fe:C ratio in the blooming region is presumingly higher, thus the rather low Fe:C ratio used refelcts the minimum amount of DFe that has to be supplied.

The vertical Fe flux (J_z) was calculated using an approach outlined in de Jong et al. (2012). The vertical DFe flux is the sum of advective Ekman pumping (left term) and diffusion (right term).

$$J_z = w[DFe]_{BWL} + \ K_z\left(\frac{\delta[DFe]}{\delta z}\right)$$

The advective Fe flux term (left) expressed by the upwelling velocity (w), which was set constant ~$1.1 * 10^{-6}$ m s^{-1} (de Jong et al., 2012), and the average dissolved Fe concentration ($[DFe]_{BWL}$) at all stations at ~ 200 m depth, contributed to 38% to the entire vertical Fe flux of 0.41 µmol m^{-2} d^{-1}. The remaining 62% are contribution of the diffusive mixing term (right term) which was derived from the DFe gradient at all stations between the surface mixed layer and ~ 200 m water depth and the vertical diffusivity, set constant at $K_z = 1 * 10^{-4}\ m^{-2}\ s^{-1}$.

Supplementary Tables

Table S1: Summary of pore water Fe and Mn flux parameters

Parameter	Unit	Fe			Mn		
Site		S1	S2	S3	S1	S2	S3
Pore w. conc. C_p	(g cm^{-3})	1.7E-07 to 9.6E-07	6.2E-08 to 8.6E-08	9.2E-08 to 1.7E-06	4.9E-08 to 1.3E-07	1.8E-08 to 4.0E-08	2.2E-08 to 2.8E-08
O_2 depth, L	(cm)	0.7	0.7	0.7	0.7	0.7	0.7
Porosity, φ		0.76	0.76	0.84	0.76	0.76	0.84
Diff. coef., D_s	(cm^2 s^{-1})	2.076E-06	2.076E-06	2.461E-06	1.877E-06	1.877E-06	2.156E-06
Bottom water [O_2]	(g cm^{-3})	1.574E-05	1.574E-05	1.700E-05	1.00E-07	1.00E-07	1.00E-07
Pore water pH		7.5	7.5	7.5	7.5	7.5	7.5
Oxidation rate, k_1	(s^{-1})	1.574E-05	1.574E-05	1.700E-05	1.00E-07	1.00E-07	1.00E-07
Flux, J	(g cm^3 s^{-1})	2.2E-13 to 1.2E-12	4.3E-15 to 6.1E-15	1.6E-13 to 2.9E-12	1.0E-13 to 2.6E-13	3.6E-14 to 8.1E-14	5.8E-14 to 7.3E-14
	(μmol m^2 d^{-1})	3.4 to 19.2	<0.1	2.5 to 44.4	1.6 to 4.1	0.6 to 1.3	0.9 to 1.1

Table S2: Fe, Mn, and Al concentrations in pore waters and sediments

Date	Station	Sample ID	Sample mid-depth (cm)	Sediment particles			Porewater	
				Fe (wt %)	Mn (ppm)	Al (wt%)	Fe (μmol kg^{-1})	Mn (μmol kg^{-1})
Feb. 2011	S1 (MC33)	AC1	0.5	3.25	635	4.77	3.0	2.421
		AC2	1.5	3.38	633	4.70	17.2	0.940
		AC3	2.5	3.31	647	4.78	110.1	0.546
		AC4	3.5	3.35	662	5.01	105.6	0.675
		AC5	4.5	3.22	649	4.65	93.5	0.520
		AC6	5.5	3.30	662	5.02	81.9	0.389
		AD1	7	-	-	-	52.6	0.271
		AD2	9	3.11	615	4.66	32.6	0.263
		AD3	11	-	-	-	27.3	0.304
		AD4	13	-	-	-	6.4	0.293
		AD5	15	3.09	612	4.69	2.5	0.209
		AD6	17	-	-	-	1.4	0.087
		AE1	19	-	-	-	0.8	0.040
		AE2	21	-	-	-	0.8	0.027
		AE3	23	-	-	-	0.7	0.028
		AE4	25	2.99	594	4.31	0.7	0.008
Feb. 2011	S2 (MC34)	AF1	0.5	3.58	627	4.77	1.5	0.585
		AF2	1.5	3.35	644	4.83	-	-
		AF3	2.5	3.24	649	4.74	1.1	0.399

		AF5	4.5	-	-	-	18.5	0.304
		AG1	6.5	3.32	672	4.94	11.1	0.264
		AG3	8.5	-	-	-	4.7	0.253
		AG5	10.5	3.24	647	4.85	14.5	0.285
		AH1	12.5	-	-	-	3.9	0.290
		AH3	14.5	3.02	595	4.32	3.8	0.285
		AH5	16.5	3.11	616	4.65	2.6	0.336
Feb. 2011	S3 (MC35)	AI1	0.5	3.43	627	4.49	1.6	0.597
		AI2	1.5	3.28	643	4.75	29.0	0.465
		AI3	2.5	3.24	642	4.75	91.1	0.373
		AI4	3.5	3.32	661	4.88	40.2	0.342
		AI5	4.5	-	-	-	37.1	0.262
		AI6	5.5	3.16	636	4.81	49.3	0.535
		AJ1	6.5	-	-	-	37.4	0.251
		AJ2	7.5	-	-	-	61.7	0.322
		AJ3	8.5	3.27	640	4.92	67.9	0.475
		AJ4	11.0	-	-	-	48.2	0.398
		AJ5	13.0	-	-	-	23.6	0.336
		AJ6	15.0	-	-	-	33.5	0.648
		AK1	17.0	3.00	593	4.57	3.8	0.181
		AK2	19.0	3.05	597	4.51	1.9	0.075
		AK3	21.0	-	-	-	1.6	0.005
		AK5	25.0	3.08	615	4.77	3.2	0.071
		AK6	27.0	-	-	-	2.9	0.052
		AL1	29.0	3.10	615	4.83	5.6	0.095

Supplementary Figures

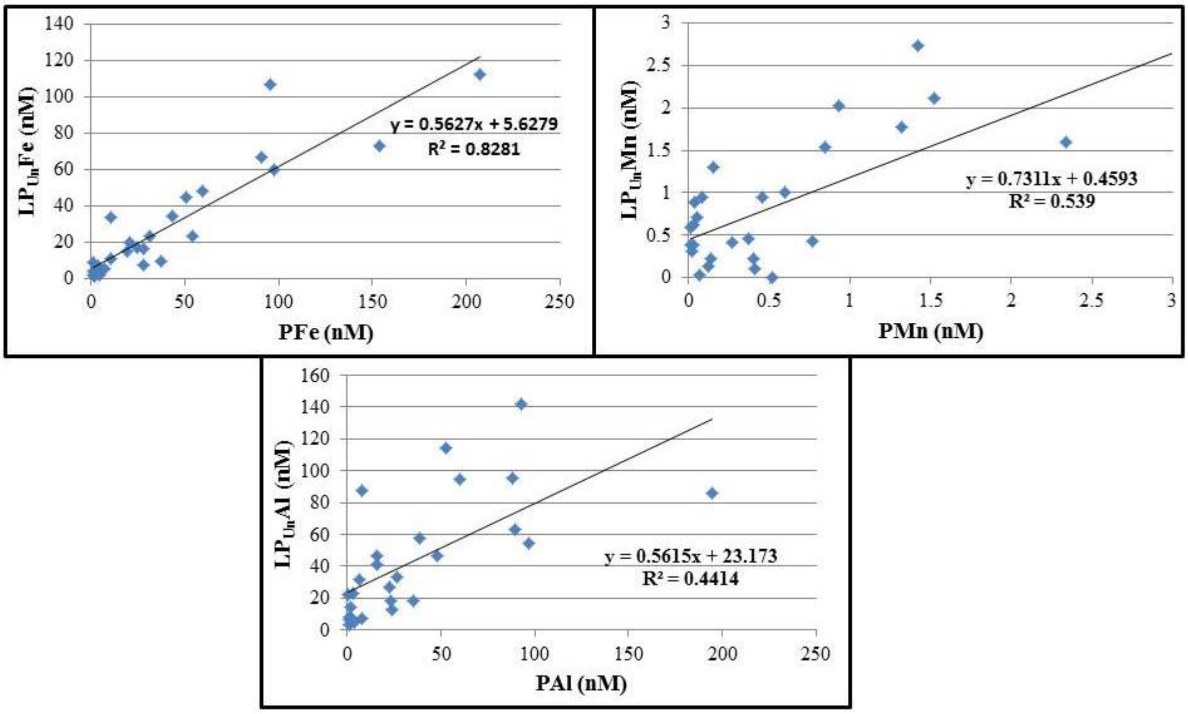

Figure S1: SAPS and OTE water sampler: Relationship of particulate trace metals from SAPS samplers (P) vs. leachable particulate trace metals from OTE water samplers (LP$_{Un}$). Data represents the entire data set collected at 20m, 50, and 100/150m.

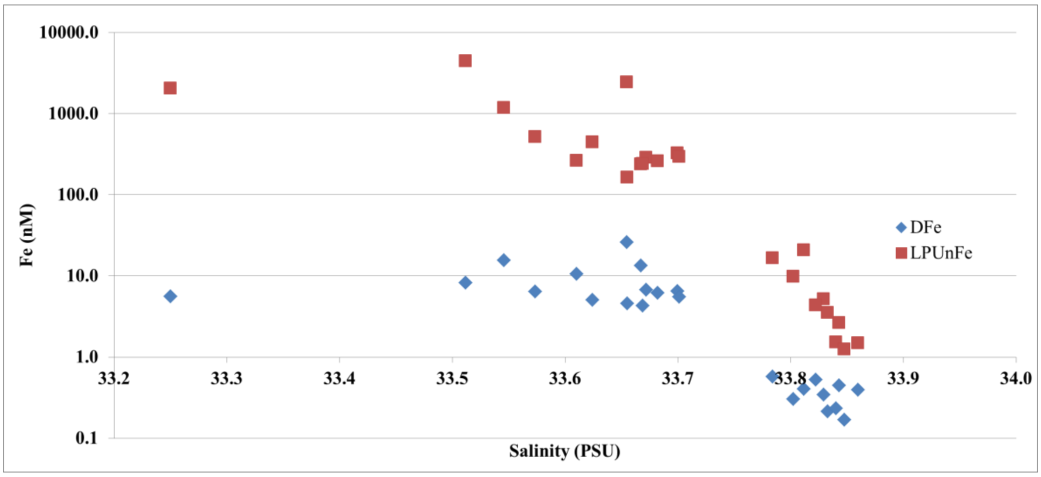

Figure ~~S1~~S2: Tow-Fish surface samples: Relationship of salinity vs. dissolved (DFe) and leachable particulate Fe (LP$_{Un}$Fe) in surface waters. The Fe concentration along the y-axis is represented in a logarithmic scale. We applied a linear regression, to validate the relationship between the DFe, $LP_{Un}Fe$ and salinity (not shown). With exception of the low salinity data point at 33.25 psu, the DFe and $LP_{Un}Fe$ vs. salinity data achieved an R^2 of 0.46 and 0.38, respectively.

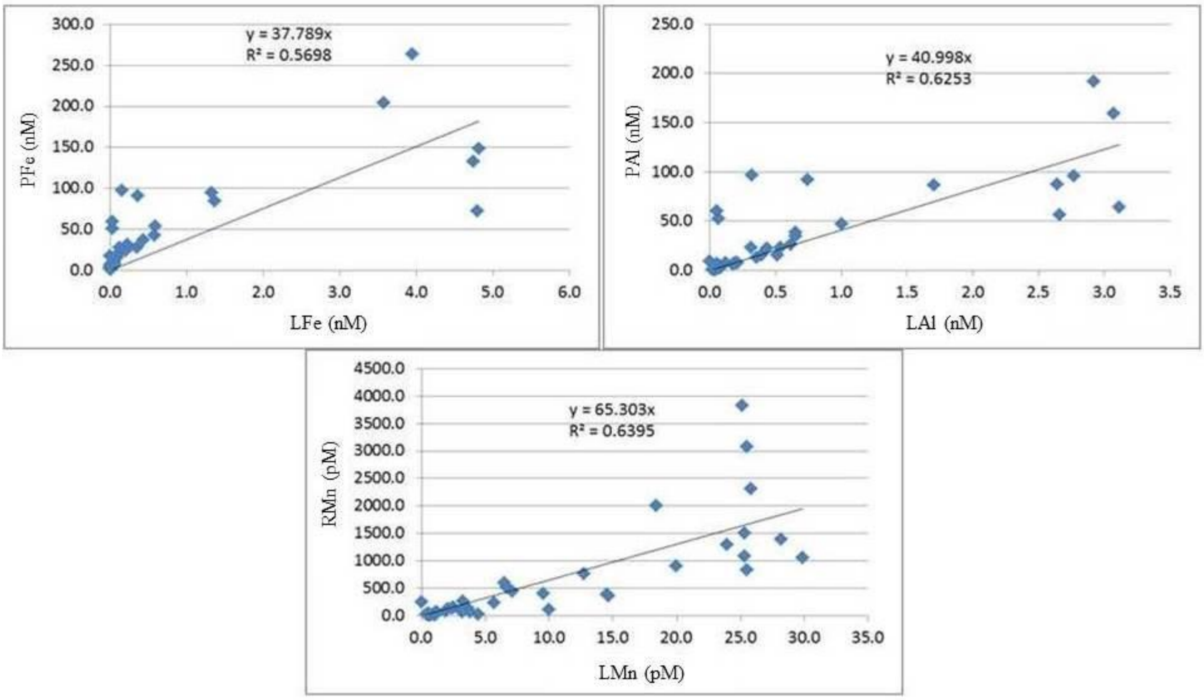

Figure ~~S2~~S3: SAPS samples: Relationship between leachable ~~particulate~~ (L~~P~~) and refractory ~~particulate~~ (R~~P~~) Fe, Mn, and Al. Due to the high proportion of RP (98.9 – 99.2% for Fe) in the particulate fraction, using the particulate fraction, P, instead of R~~P~~ changes the linear regression with L~~P~~ just very little.

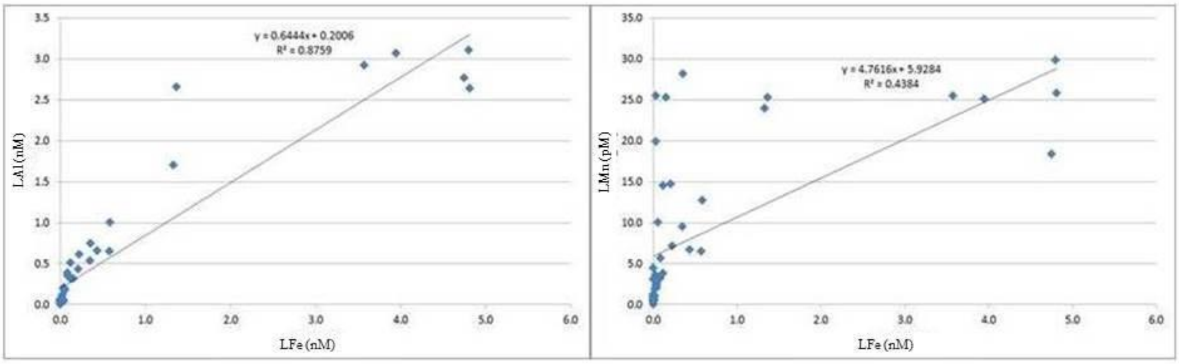

Figure ~~S3~~S4: SAPS samples: Relationship between leachable ~~particulate~~ Fe, Mn and Al.

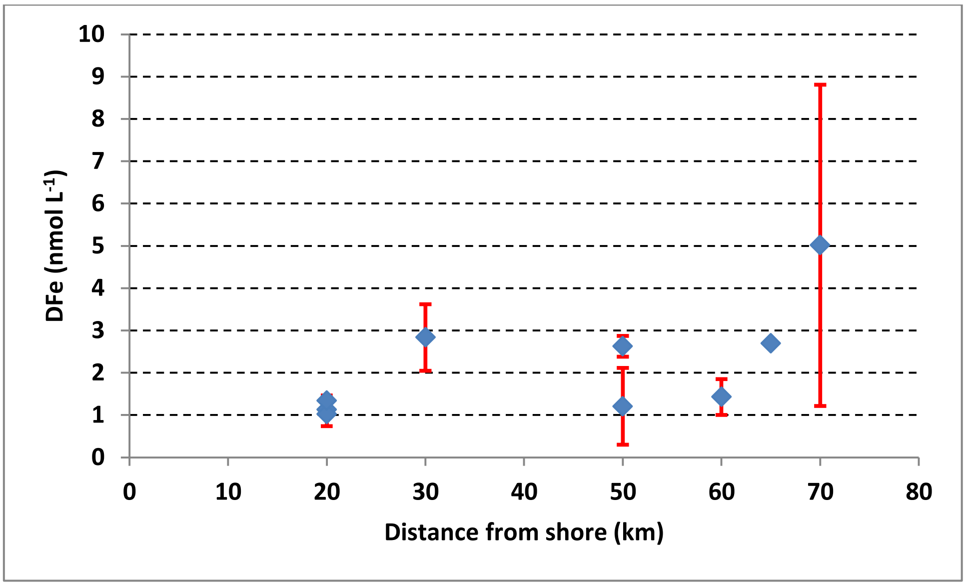

Figure ~~S4~~S5: OTE-water sampler: Average dissolved Fe concentration between 100 and 400 m water depth versus distance to the coast line of South Georgia in kilometre.

References

Boudreux, B. P. and Scott, M. R.: A model for the diffusion-controlled growth of deep-sea manganese nodules, Americ. J. Sc., 278, 903-929, 1978.

de Jong, J., Schoemann, V., Lannuzel, D., Croot, P., de Baar, H. J. W., and Tison, J. L.: Natural iron fertilization of the Atlantic sector of the Southern Ocean by continental shelf sources of the Antarctic Peninsula, J. Geophys. Res., 117, 1-25, 2012.

Ho, T.-Y., Quigg, A., Finkel, Z. V., Milligan, A. J., Wyman, K., Falkowski, P. G., and Morel, F. M. M.: The elemental composition of some marine phytoplankton, J. Phycol., 39, 1145-1159, 2003.

Homoky, W. B., John, S. G., Conway, T. M., and Mills, R. A.: Distinct iron supply and isotope signatures from marine sediment dissolution, Nat. Commun., 4:2143, 2013.

Homoky, W. B., Severmann, S., McManus, J., Berelson, W. M., Riedel, T. E., Statham, P. J., and Mills, R. A.: Dissolved oxygen and suspended particles regulate the benthic flux of iron from continental margins, Mar. Chem., 134–135, 59-70, 2012.

John, S. G., Mendez, J., Moffett, J. W., and Adkins, J.: The flux of iron and iron isotopes from San Pedro Basin sediments, Geochim. Cosmochim. Act., 93, 14-29, 2012.

Kagaya, S., Maebe, E., Inoue, Y., Kamichatani, W., Kajiwara, T., Yanai, H., Saito, M., and Tohda, K.: A solid phase extraction using a chelate resin immobilizing carboxymethylated pentaethylenehexamine for separation and preconcentration of trace elements in water samples, Talanta, 79, 146-152, 2009.

Ma, S., Tao, Z., Yang, X., Yu, Y., Zhou, X., M, W., and Li, Z.: Estimation of marine primary productivity from satellite-derived phytoplankton absorption data, IEEE J-STARS, 7, 3084-3092, 2014.

McManus, J., Berelson, W. M., Severmann, S., Johnson, K. S., Hammond, D. E., Roy, M., and Coale, K. H.: Benthic manganese fluxes along the Oregon-California continental shelf and slope, Cont. Shelf Res., 43, 71-85, 2012.

Millero, F. J., Sotolongo, S., and Izaguirre, M.: The oxidation kinetics of Fe(II) in seawater, Geochim. Cosmochim. Act., 51, 793-801, 1987.

Raiswell, R. and Anderson, T. F.: Reactive iron enrichment in sediments deposited beneath euxinic bottom waters: constraints on supply by shelf recycling, Geological Society, London, Special Publications, 2005.

Rapp, I., Schlosser, C., Rusiecka, D., Gledhill, M., and Achterberg, E. P.: Automated preconcentration of Fe, Zn, Cu, Ni, Cd, Pb, Co, and Mn in seawater with analysis using high-resolution sector field inductively-coupled plasma mass spectrometry, Anal. Chimi. Acta, 976, 1-13, 2017.

Strzepek, R., Maldonado, M. T., Hunter, K. A., Frew, R. D., and Boyd, P. W.: Adaptive strategies by Southern Ocean phytoplankton to lessen iron limitation: Uptake of organically complexed iron and reduced cellular iron requirements, Limnol. Oceanogr., 56, 1983-2002, 2011.

Twining, B. S., Baines, S. B., Fisher, N. S., and Landry, M. R.: Cellular iron contents of plankton during the Southern Ocean Iron Experiment (SOFeX), Deep-Sea Res. I, 51, 1827-1850, 2004.